

Chapter 1

Coherent control and decoherence of charge states in quantum dots

Paweł Machnikowski

*Institute of Physics, Wrocław University of Technology,
50-370 Wrocław, Poland,
Pawel.Machnikowski@pwr.wroc.pl*

This Chapter contains a review of the recent results, both experimental and theoretical, related to optical control of carriers confined in semiconductor quantum dots. The physics of Rabi oscillations of exciton and biexciton occupations, as well as time-domain interference experiments are discussed. Next, the impact of carrier-phonon interaction in a semiconductor structure is described and modern methods of theoretical description of the carrier-phonon kinetics and of the resulting dephasing are presented.

1.1. Introduction

The progress of semiconductor technology that took place in the 80s and 90s of the last century, in particular the rapid development of epitaxy and lithography techniques, has allowed physicists to manufacture and study structures in which carriers are confined to a small volume in space (tens of nanometers or even less).¹ In this way quantum dots (QDs), that is, artificial structures (boxes) containing a few particles with quantized energy levels, have been produced. Because of the similarity to natural atoms, such structures are also referred to as artificial atoms. However, the properties of QDs are more flexible in comparison with atoms: their shapes, size and various other features can be engineered at the stage of manufacturing by modifying the technological conditions and the number of confined electrons can be changed under laboratory conditions (e.g. by applying an external voltage) within a wide range of values.

Parallel to the laboratory investigations, a rapid process of miniaturization of commercial semiconductor structures (e.g., computer chips) took

place. At this moment, the state-of-the-art commercially available microchips, manufactured using the immersion photolithography technique, are built of elements whose size can be reduced down to the 90 nm diffraction limit. The introduction of the 45 nm process is announced for 2007 or early 2008 and the implementation of the 16 nm technology is envisaged in the time frame 2013-14.^a Thus, the characteristic size of elements in the microchips of our standard computer equipment has dropped below the size of the first QDs obtained in laboratories 20 years ago and rapidly approaches the size of the smallest structures described in today's research papers.

This progress of manufacturing technology is accompanied by a rapid development of optical spectroscopy. Currently, it is possible to study the optical properties of a single QD and to coherently control the evolution of a single carrier or a pair of carriers (electron-hole pair) in such a structure. Many experimental schemes of quantum optics have been implemented on QDs. Moreover, certain procedures relying on the specific structure of the energy levels of these artificial semiconductor structures have been demonstrated, which have no counterpart in atomic systems. These experimental achievements have motivated theoretical proposals for sophisticated quantum-optical schemes that may lead, for instance, to optical control of a single electron spin in a QD.

The goal of this chapter is twofold: First, to introduce the reader into the fascinating world of modern optical experiments on semiconductor quantum dots and to the astonishingly simple, yet nontrivial, theory underlying the phenomena observed in the labs on the fundamental, quantum-optical level. Second, to give a review of some more sophisticated theoretical methods that allow one to include the interaction with the lattice vibration modes (phonons) which are specific to semiconductor systems.

1.2. Essential properties of quantum dots

Quantum dots are semiconductor structures in which the carrier dynamics is restricted in all three dimensions to the length scales of several or a few tens of nanometers.^{2,3} Various structures that have this property may be obtained by a variety of methods.

One of the most widely used techniques is the Stransky-Krastanov self-assembly. When a semiconductor compound is epitaxially (layer by layer) grown on a substrate with a different lattice constant (the InAs/GaAs pair

^aInternational Technology Roadmap for Semiconductors (www.itrs.net).

is a typical example) each new layer must be squeezed to match the lattice constant of the substrate. At some point (at about 1.7 monolayers for InAs/GaAs) it is energetically favorable for the epitaxial layers to restructure into a system of islands, which increases the free surface but relaxes strain.⁴ The sample is then covered with the substrate material, leading to lens-shaped (or, sometimes, pyramidal) nanostructures as in Fig. 1.1a.⁵ In general, the band edges of the nanostructure material are offset with respect to those of the substrate. Here we will only discuss structures as those in Fig. 1.1b-d, where the conduction band edge is shifted down and the valence band edge is shifted up, so that both electrons and holes are bound in the QD structure.

Another type of structures commonly used in the optical experiments are thickness fluctuations of a thin epitaxial layer of a semiconductor (so called quantum well) placed between thick structures of different semiconductor with a wider band gap. Here, again, the band edge offset leads to localization of carriers within the quantum well layer. If the epitaxial growth of the quantum well layer has been stopped after the formation of a new monolayer started, the quantum well has one-monolayer thickness fluctuations which weakly localize the carriers.

The QD nanostructures are typically 2–3 orders of magnitude larger than atoms. However, the effective mass of carriers in a semiconductor is often considerably lower than the free electron mass (e.g. $m^* = 0.07m_0$ in GaAs), and this degree of confinement is sufficient for quantization of carrier energies with electron inter-level spacing reaching 100 meV in self-assembled structures. This is definitely enough to resolve the states spectrally and to neglect thermal transitions to the excited states even at moderate temperatures. Therefore, we will restrict the discussion to the ground state of each kind of carriers.

The exact properties of the quantum states in a QD, e.g., the geometry of wave functions or Coulomb interaction between the confined carriers, may be found, e.g., by tight-binding or pseudopotential calculations. For lens-shaped QDs, a simple 2-dimensional harmonic model² has been shown to be a very good approximation.⁶ The states of an interacting few-particle system may then be found by numerical configuration–interaction techniques.^{7,8} However, these details are irrelevant for the discussion on the general quantum-optical level. Whenever a specific model is necessary (Secs. 1.6 and 1.7) we will use simple Gaussian wave functions. Also in these cases, the results do not depend essentially on this choice.

Even with the restriction to the lowest orbital states, the structure of

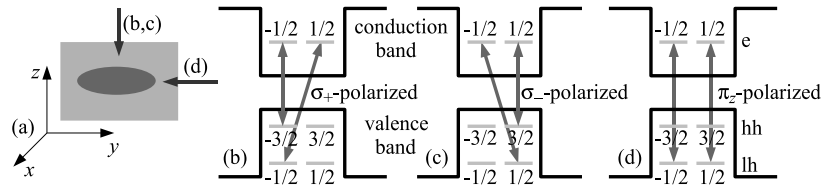


Fig. 1.1. (a) Schematic plot of a QD. The xy plane is referred to as the structure plane, while z is called growth direction and corresponds to the (approximate) symmetry axis of the structure. The arrows show the incidence of light corresponding to the three diagrams b-d. (b-d) The diagrams showing the transitions allowed by selection rules in a III-V QD, induced by light circularly polarized in the structure plane (b: right-polarized, c: left-polarized) and by light linearly polarized along z (d).

energy levels and allowed optical transitions in a QD becomes quite complicated if the angular momenta of carriers are taken into account. The valence band in III-V semiconductors is composed of p-type atomic orbitals (orbital angular momentum 1), yielding six quantum states (taking spin into account) for each quasi-momentum \mathbf{k} . Due to considerable spin-orbit coupling the orbital angular momentum and spin are not separate good quantum numbers and the valence band states of a bulk crystal must be classified by the total angular momentum and its projection on a selected axis. Thus, the valence band is composed of three sub-bands corresponding to two different representations of the total angular momentum J . Out of these, the two states with $j = 1/2$ form a subband which is split-off by the spin-orbit interaction. The other four states with $j = 3/2$ are degenerate in a bulk crystal at $\mathbf{k} = 0$ but this degeneracy is lifted by size quantization and strain in a QD structure, with the heavy hole (hh) subband (angular momentum projection on the symmetry axis ($m = \pm 3/2$) lying above the light hole (lh) subband ($m = \pm 1/2$) in all known structures. The fundamental optical excitation of a QD consists in transferring optically an electron from the highest confined state in the valence band (thus leaving a hole) to the lowest confined state in the conduction band. The interacting electron-hole pair created in this way is referred to as exciton (lh-exciton or hh-exciton, depending on the kind of a hole involved). Angular momentum selection rules restrict the transitions allowed for a given propagation direction and polarization of the light beam, as depicted in Fig. 1.1. For instance, according to the selection rules represented in Fig. 1.1b, a right circularly polarized (σ_+ -polarized) laser beam can only create an exciton with total momentum $+1$, referred to as “ σ_+ exciton”, in accordance with the angular

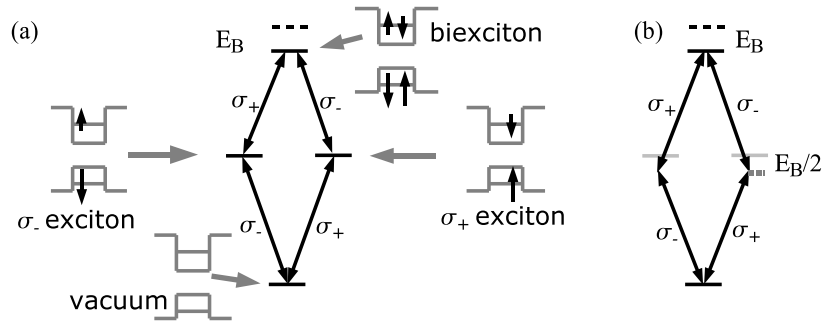


Fig. 1.2. (a) The four states of the heavy-hole biexciton system and the optical transitions between them. The band diagrams show the particles forming each state. The arrows in the valence band represent holes. (b) Schematic representation of the two-photon resonance between the ground state and the biexciton state, achieved with a properly tuned linearly polarized laser beam. Note that the single exciton transitions are forbidden.

momentum conservation (removing an electron with the angular momentum m is equivalent to the creation of a hole with the angular momentum $-m$). Similarly, a σ_- -polarized (left circularly polarized) beam creates only a “ σ_- exciton” with the angular momentum -1 . Although there are still two transitions allowed for a given circular polarization they can easily be distinguished since the lh states are well separated energetically from the lowest hh states.

In appropriately doped structures, QDs in the ground state of the system may be occupied by electrons. An optical excitation in this case corresponds to a transition between a single electron state and a negative trion state, i.e., the state of two electrons and one hole confined in a QD. From the Pauli exclusion principle it is clear that this transition is possible only if the state which is to be occupied by the photo-created electron is free. Hence, in the situation of Fig. 1b, a heavy hole trion may be created if the dot is initially occupied by a “spin up” ($m = +1/2$) electron but not if the electron in the dot is in the “spin down” ($m = -1/2$) state. This suppression of the optical transition depending on the spin of the electron in the QD is referred to as Pauli blocking and has been indeed observed experimentally.⁹

After exciting an electron from the heavy hole band with a σ_+ -polarized laser beam ($m = -3/2 \rightarrow -1/2$), as in Fig. 1.1b, it is still possible to transfer also the $m = +3/2$ electron to the $m = +1/2$ conduction band state using σ_- -polarized light (Fig. 1.1c). Thus, if the optical processes

are spectrally restricted to heavy holes (as is the case in most experiments) there are four optically active states linked by allowed optical transitions as shown in Fig. 1.2a. The highest state, with two electrons and two holes present in the QD, is treated as composed of two electron-hole pairs and is called a biexciton. The Coulomb (dipole-dipole) interaction between the two excitons shifts the energy of the biexciton state¹⁰ by the binding energy E_B , so that the exciton–biexciton transitions are non-degenerate with the ground state–exciton transitions. In this way, all four transitions in the diagram can be distinguished either spectrally or by polarizations.

1.3. Coherent control: experimental state of the art

The recent progress in ultrafast spectroscopy of semiconductor systems^{11,12} made it possible to control and probe the quantum states of carriers confined in a QD on femtosecond time scales. In particular, high degree of control over carrier occupations in various kinds of QD structures has been demonstrated. One kind of an experiment consists in measuring the average occupation of the QD after a pulse of fixed length but variable amplitude. The QD occupation is defined as the probability of finding an exciton in the QD after the laser pulse, calculated as the fraction of cases in which an exciton was created over a large number of repetitions of the experiment. Within the linear absorption theory, the excitation (the QD occupation) grows proportionally to the pulse intensity. Obviously, this growth cannot be unlimited. When the occupation of the excited level is sufficiently large the spontaneous and induced emission processes suppress further increase of the occupation. Here, we are interested in the coherent limit, where the evolution is induced by a strong (essentially classical) laser field, inducing large occupation changes over time scales much shorter than the spontaneous emission time. Then, the system is driven from the ground to the excited state in a coherent way, and then back to the ground state via a coherently induced emission process. As a result, in an ideal case, the final occupation after a pulse should show sinusoidal oscillations between 0 and 1 as a function of the square root of pulse intensity (referred to as *pulse area* – see Sec.1.4.2). Such oscillations, known as pulse area dependent Rabi oscillations, have been indeed observed in a range of experiments on single QDs.^{13–16} Similar effect can also be observed in ensembles of QDs.¹⁷

In Fig. 1.3a we show the results of such an experiment, performed with a single QD-based photodiode structure.^{15,16,18} In this experiment the QD is placed in an electric field between a pair of electrodes (Fig. 1.3c).

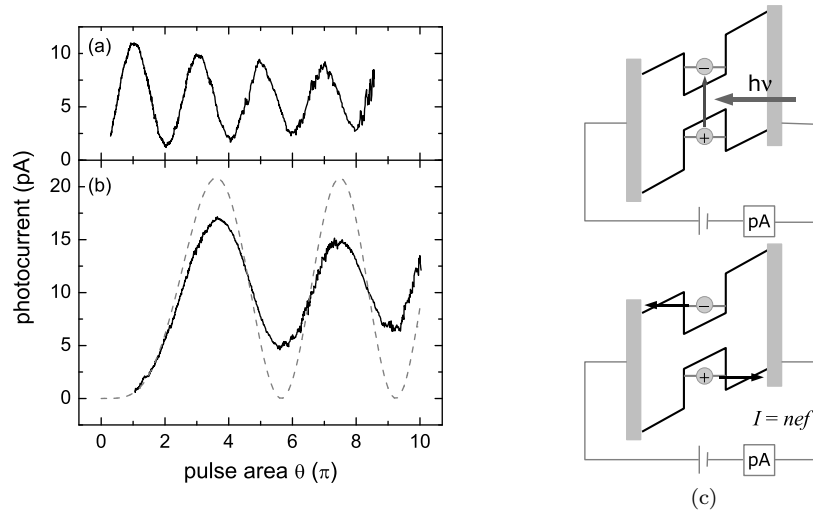


Fig. 1.3. (a) Pulse area dependent Rabi oscillations. (b) Two-photon Rabi oscillations. Solid line: experiment, dashed line: theory (without dephasing), assuming a sech pulse shape with a pulse length of 2.3 ps and biexciton binding energy $E_B = 2.7$ meV. Reprinted from Ref. 18, S. Stuffer *et al.*, Phys. Rev. B **73**, 125304 (2006), ©American Physical Society 2006. (c) A schematic explanation of the functionality of the QD photodiode.

Each electron-hole pair generated by the optical excitation contributes to the photocurrent in the structure. If the laser pulse repetition rate is f (typically in kHz–MHz range) and the average QD occupation for a given pulse area is n , then the repeated pulsing results in a current $I = nef$. In this way, the Rabi oscillations of the average exciton number are reflected in the oscillating form of the photocurrent as a function of the pulse area, which provides a means of detection much more efficient than optical ones. These oscillations are clearly seen in Fig. 1.3a, although some damping, due to dephasing, is also visible.

Apart from the coherent control of exciton occupations, it has also been shown that phase control of carrier states in QDs is possible. A laser pulse detuned from the exciton resonance cannot induce real transitions and, therefore, does not change occupations. Nonetheless, as shown in an optical experiment with interface fluctuation QDs,¹⁹ it can shift the energy levels via the AC (optical) Stark effect and affect the phases in a quantum superposition of empty dot and single-exciton states. Another way to control the phases is to drive the system with a slightly detuned laser

pulse, which leads to a combination of occupation and phase evolution²⁰ (see Sec. 1.4.2). In this case, phase effects can be observed in the form of Ramsey interference fringes.²¹

It is possible to see in an experiment that the quantum state of an electron-hole pair in a QD maintains its phase coherence long after the laser pulse has been switched off. To this end, one splits the pulse into two parts. If the phase of the quantum state in the QD were random when the second pulse arrives the phase of the latter would be irrelevant. On the contrary, in the experiment one observes oscillations of the final QD occupation as a function of the relative phase shift between the two pulses^{14,22,23} (the phase is shifted by tuning the delay between the pulses with a sub-femtosecond accuracy, that is, by a fraction of the optical oscillation period). Such an effect is referred to as time-domain interference, since it may be interpreted in terms of interference between the probability amplitudes for exciting the QD with the first or with the second pulse. A formal treatment of this class of experiments will be given in Sec. 1.4.3.

Apart from the fact that such interference experiments demonstrate coherent phase-sensitive quantum control with an amazingly precise timing, they are also of interest from a more general point of view. Obviously, in spite of the wave-like behavior manifested by the interference effect, a single measurement of the QD occupation always yields either 0 or 1, demonstrating the particle-like nature of the exciton. Thus, the time-domain interference experiments on QDs demonstrate quantum complementarity between the particle-like nature of an exciton and its ability to show quantum interference.²⁴

Controlling a single quantum degree of freedom (an exciton) is just the first step towards large-scale nano-optoelectronic and quantum computing applications. The next step towards more complex implementations is to include coupling between two or more individual quantum subsystems. The simplest experimental realization of such a composite system is a biexciton. As explained in Sec. 1.2, due to the Coulomb interaction between the two excitons, the excitation energy of an exciton in the presence of the other one is different than in its absence. Thus, these two transitions can be addressed individually. Together with the polarization dependence of the allowed transitions (selection rules, see Sec. 1.2), this allows one to excite, say, the σ_+ exciton if and only if the σ_- exciton is present. Such a conditional control procedure was indeed performed in an experiment,²⁵ where Rabi oscillations on the exciton–biexciton transition were demonstrated. If the two excitons are viewed as quantum bits (with 0 and 1 corresponding

to their presence or absence in the QD) then such a conditional excitation constitutes an implementation of the controlled-NOT gate which is fundamental for quantum computing.²⁶ Such a controlled-NOT gate was indeed implemented experimentally in a QD system.²⁵ In a similar way it is possible to coherently manipulate a biexciton system in two coupled QDs (with one exciton localized in each dot).²⁷

It is interesting to see what happens if the frequency ω of a linearly polarized laser beam is chosen such that the energy of two photons matches the biexciton energy, $2\omega = 2E - E_B$, while the single-exciton transitions are detuned by $E_B/2$ (Fig.1.2b). A linearly polarized pulse is a superposition of two circularly polarized components, so that both exciton transitions are allowed by the selection rules but neither of them satisfies the energy conservation. Perturbation theory would predict that the occupation of the biexciton state should grow proportionally to the square of the pulse intensity (that is, to the 4th power of the pulse area), as a result of a two-photon absorption process. Experimental results¹⁸ presented in Fig. 1.3b indeed show such a behavior for low pulse intensities. However, beyond this perturbative regime, a pattern of two-photon pulse area dependent Rabi oscillations between the ground and biexciton states develops, which become almost periodic for large pulse intensities. The theory of such coherent phenomena in the biexciton system will be presented in Sec. 1.5.

1.4. Quantum dot as a two-level system

Let us now proceed to a theoretical description of the quantum evolution of carriers confined in a QD and subject to a laser field. We will start with the simplest situation when the QD is driven by a circularly polarized laser beam (say, σ_+) tuned to the fundamental heavy hole transition, as in Fig. 1.1a (vertical arrow). Then, only two states are involved in the evolution: the ground state (empty dot), denoted by $|0\rangle$, and the σ_+ exciton state, denoted $|1\rangle$ (see also Fig. 1.2a). Therefore, one effectively deals with a very simple two-level system.

1.4.1. General considerations

The discussion of such systems is made particularly transparent by introducing the concept of the Bloch sphere (actually, a ball). The state (pure or mixed) of such a system is represented by a density matrix: a 2×2 , hermitian, and positive definite operator with unit trace. Any such operator

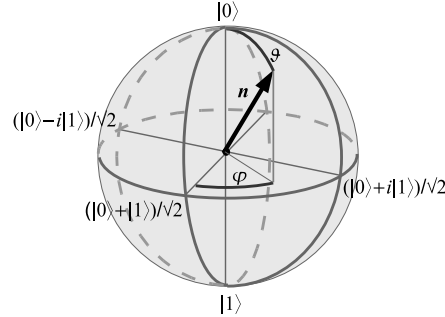


Fig. 1.4. The Bloch sphere.

can be written in the form

$$\rho = \frac{1}{2}(\mathbb{I} + \mathbf{n} \cdot \boldsymbol{\sigma}), \quad (1.1)$$

where \mathbf{n} is a real three-dimensional vector with $n = |\mathbf{n}| \leq 1$, \mathbb{I} is the unit operator, and $\boldsymbol{\sigma}$ is the vector of Pauli matrices in the basis $|0\rangle, |1\rangle$. Thus, the state of a two-level system is represented in a unique way by a unit ball in a three-dimensional real space (Fig. 1.4). Since $\text{Tr} \sigma_i = 0$, $\text{Tr} \mathbb{I} = 2$, and $(\mathbf{n} \cdot \boldsymbol{\sigma})^2 = n^2 \mathbb{I}$, one finds $\text{Tr} \rho^2 = n^2$, so that pure states (represented by projectors) correspond to unit vectors \mathbf{n} and are mapped to the surface of the ball. It is easy to see that the point with spherical coordinates (ϑ, φ) represents the state vector $\cos(\vartheta/2)|0\rangle + e^{i\varphi} \sin(\vartheta/2)|1\rangle$.

The electric field of the laser beam is conveniently written as $\mathcal{E}(t) \cos(\omega t - \phi)$, where ω is the frequency of the light, ϕ is the phase of the pulse and $\mathcal{E}(t)$ is the envelope of the pulse, varying slowly compared to the oscillations of the optical field. The state of the system $|\Psi\rangle$ evolves according to the Schrödinger equation

$$i\hbar \frac{d}{dt} |\Psi\rangle = H |\Psi\rangle, \quad (1.2)$$

with the Hamiltonian

$$H = E|1\rangle\langle 1| + \mathcal{E}(t - t_a) \cos[\omega(t - t_a) - \phi] (\mu|0\rangle\langle 1| + \mu^*|1\rangle\langle 0|), \quad (1.3)$$

where E is the energy of the interband transition in the QD, μ is the off-diagonal (interband) matrix element of the electric dipole moment (between the two relevant states), and we allow the pulse to arrive at an arbitrary time t_a . By a proper choice of the phase of the state $|1\rangle$ it is possible to have μ real, which will be assumed in the following. We will use the shorthand notation $f(t) = \mu \mathcal{E}(t)$.

In the absence of the driving, the phase of the state $|1\rangle$ rotates with the frequency E/\hbar which is of the order of fs^{-1} . One gets rid of this trivial fast dynamics by describing the system in the frame rotating with the same frequency. This is similar to a transition to the interaction picture except that, for practical reasons, it is convenient to perform the transformation with the laser frequency ω instead of the system frequency E/\hbar (these two frequencies are close to each other). Thus, we perform the transformation

$$|\tilde{\Psi}\rangle = U_r|\Psi\rangle, \quad U_r = \exp(i\omega t|1\rangle\langle 1|).$$

Using Eq. (1.2) one easily finds the evolution equation for the redefined states in the form $i\hbar|\dot{\tilde{\Psi}}\rangle = \tilde{H}|\tilde{\Psi}\rangle$, with the Hamiltonian

$$\begin{aligned} \tilde{H} &= -\hbar\omega|1\rangle\langle 1| + U_r H U_r^\dagger \\ &= -\Delta|1\rangle\langle 1| + \frac{1}{2}f(t-t_a) \left[\left(e^{-i\omega t_0 - i\phi} + e^{-i\omega(2t-t_0) + i\phi} \right) |0\rangle\langle 1| \right. \\ &\quad \left. + \left(e^{i\omega t_0 + i\phi} + e^{i\omega(2t-t_0) - i\phi} \right) |1\rangle\langle 0| \right], \end{aligned} \quad (1.4)$$

where $\Delta = \hbar\omega - E$ is the detuning of the laser beam from the transition energy.

The next essential step is to note that the natural frequency scale of the system evolution is set by the detuning Δ and by the pulse amplitude $f(t)$ and is many orders of magnitude smaller than the optical frequency ω . Therefore, the quickly oscillating terms ($\sim e^{2i\omega t}$) are strongly off-resonant and will have very little impact on the system evolution. Therefore, they can be neglected, which leads to the rotating wave approximation (RWA).²⁸ As a result, one obtains the following RWA Hamiltonian

$$\begin{aligned} H_{\text{RWA}} &= -\Delta|1\rangle\langle 1| + \frac{1}{2}f(t-t_a) \left(e^{-i(\omega t_0 + \phi)} |0\rangle\langle 1| + e^{i(\omega t_0 + \phi)} |1\rangle\langle 0| \right) \\ &= -\Delta|1\rangle\langle 1| + \frac{1}{2}f(t-t_a)\hat{\mathbf{u}} \cdot \boldsymbol{\sigma}, \end{aligned} \quad (1.5)$$

where $\hat{\mathbf{u}} = [\cos(\omega t_a + \phi), \sin(\omega t_a + \phi), 0]$.

1.4.2. Pulse area dependent Rabi oscillations

Let us start with applying the formalism to the Rabi oscillations described in Sec. 1.3. First, assume that the pulse is resonant with the optical transition in the QD, that is, $\Delta = 0$. In this case, the evolution operator generated by the RWA Hamiltonian (1.5) can be found analytically. Indeed, in the resonant case the Hamiltonians at different times commute

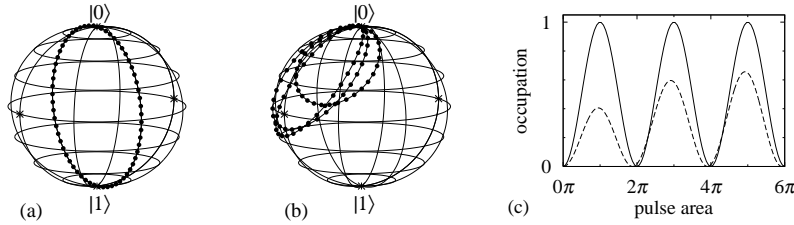


Fig. 1.5. (a) Pulse-area dependent Rabi oscillations at the resonance. The points represent final system states for different pulse areas $\alpha \in (0, 2\pi)$ with a step of $\Delta\alpha = 0.1$. (b) Pulse-area dependent Rabi oscillations off resonance. The points represent final system states for different pulse areas $\alpha \in (0, 6\pi)$ with a step of $\Delta\alpha = 0.2$. (c) The occupation of the state $|1\rangle$ as a function of the pulse area for resonant (solid) and non-resonant (dashed) driving.

with one another, so that the evolution operator may be written as

$$U(t) = \exp\left[\frac{1}{2}\Phi(t)\hat{\mathbf{u}} \cdot \boldsymbol{\sigma}\right] = \cos\frac{\Phi(t)}{2}\mathbb{I} - i\sin\frac{\Phi(t)}{2}\hat{\mathbf{u}} \cdot \boldsymbol{\sigma}, \quad (1.6)$$

where $\Phi(t) = \int_{t_0}^t d\tau f(\tau)$, t_0 is the initial time of the evolution, and the last identity is easily proven by expanding the exponent in a series and collecting the odd- and even-order terms using the identities $(\hat{\mathbf{u}} \cdot \boldsymbol{\sigma})^{2m} = \mathbb{I}$ and $(\hat{\mathbf{u}} \cdot \boldsymbol{\sigma})^{2m+1} = \hat{\mathbf{u}} \cdot \boldsymbol{\sigma}$ for any natural number m . We will always assume that this time is before any pulses were switched on, so that one can set $t_0 \rightarrow -\infty$. The value of $\alpha \equiv \Phi(\infty)$ is called the pulse area and determines the unitary transformation of the system state performed by the complete pulse. One speaks of π -pulses, $\pi/2$ pulses etc., referring to the value of the pulse area.

Starting from the ground system state $|0\rangle$ one obtains, after switching the pulse off,

$$|\tilde{\Psi}\rangle = U(\infty)|0\rangle = \cos\frac{\alpha}{2}|0\rangle - ie^{i\phi}\sin\frac{\alpha}{2}|1\rangle. \quad (1.7)$$

The occupation of the state $|1\rangle$ is, therefore,

$$|\langle 1|\Psi\rangle|^2 = |\langle 1|\tilde{\Psi}\rangle|^2 = \sin^2\frac{\alpha}{2}$$

and indeed oscillates between 0 and 1 as a function of the pulse area α . The final system states for a set of values of α in this resonant case are shown in Fig. 1.5a. Let us note here that the final state is determined by a simple function of just one quantity, the pulse area, and is independent of any details of the pulse shape. This fact is known as the area theorem.

Off resonance (for $\Delta \neq 0$), the evolution can be found in a closed analytical form only for rectangular pulse envelopes $f(t)$.²⁹ Instead of performing this simple exercise, let us look at the evolution for a family of Gaussian pulses

$$f(t) = \frac{\hbar\alpha}{\sqrt{2\pi}\tau_p} e^{-\frac{1}{2}\left(\frac{t}{\tau_p}\right)^2} \quad (1.8)$$

obtained by (also very simple) numerical integration of the Schrödinger equation (1.2), shown in Fig. 1.5b (see also Ref. 20). In the detuned case, the system does not reach the $|1\rangle$ state. Instead, the state is rotated around a tilted axis and the final state does not show periodicity as a function of the pulse area. The difference between the resonant and non-resonant case is also visible in the dependence of the final occupation of the state $|1\rangle$ (Fig. 1.5c).

1.4.3. Time-domain interference

Another experiment that can easily be explained based on the two level model is that of time domain interference. As discussed in Sec. 1.3, such experiments are performed with two laser pulses selectively tuned to the exact resonance with one of the two fundamental optical transitions. The pulses are generated by splitting a single laser pulse and delaying one part with respect to the other. In this way, the two pulses are phase-locked, i.e., their relative phase is definite and determined by the delay time τ . The first pulse arrives at $t_a = 0$ and prepares the initial superposition state. In a usual two-slit (space-domain) experiment, this would correspond to splitting the particle path. The second pulse arrives at $t_a = \tau$. This pulse plays the role of “beam merger” providing, at the same time, a phase shift between the “paths”.

The Hamiltonian describing the system driven by the two pulses is obtained by an obvious generalization of Eq. (1.5).

$$H = \frac{1}{2}f_1(t)(|0\rangle\langle 1| + |1\rangle\langle 0|) + \frac{1}{2}f_2(t - \tau)(e^{-i\omega\tau}|0\rangle\langle 1|e^{i\omega\tau}|1\rangle\langle 0|), \quad (1.9)$$

where $f_i(t)$ are the envelopes of the two pulses and we have set $\phi = 0$. The pulses do not overlap in time so that the evolution can be split into two independent stages.

In an experiment, the system is initially in the state $|0\rangle$. The first pulse is a $\pi/2$ pulse that performs the transformation $U_1 = (\mathbb{I} - i\sigma_x)/\sqrt{2}$. This

pulse leaves the system in the equal superposition state

$$|\psi\rangle = \frac{|0\rangle - i|1\rangle}{\sqrt{2}}. \quad (1.10)$$

The second pulse is again a $\pi/2$ pulse,

$$U_2 = \frac{1}{\sqrt{2}}(\mathbb{I} - i\hat{\mathbf{n}} \cdot \boldsymbol{\sigma}), \quad (1.11)$$

where $\hat{\mathbf{n}} = [\cos\omega\tau, \sin\omega\tau, 0]$, as follows from the general discussion in Sec. 1.4.1. After this pulse, the average number of excitons in the dot is

$$N(\phi) = |\langle 1|U_2|\psi\rangle|^2 = \frac{1}{2}(1 - \cos\omega\tau),$$

and changes periodically between $N_{\min} = 0$ and $N_{\max} = 1$ as a function of the delay time τ , thus producing an interference pattern.

The quality of the interference pattern is quantified in terms of visibility of interference fringes

$$\mathcal{V} = \frac{N_{\max} - N_{\min}}{N_{\max} + N_{\min}}.$$

The amplitude (visibility) of the fringes in an ideal experiment is $\mathcal{V} = 1$ for $\pi/2$ pulses, i.e., for an equal superposition state in between the pulses. Otherwise, some *a priori* information on the superposition state can be inferred and the visibility is reduced. Reduction of visibility occurs also if some information on the system state between the pulses (analogous to *which way* information) has been extracted either intentionally, in a controlled experiment (see Sec.1.5.2), or as a result of uncontrolled dephasing.²⁴

1.5. Beyond the two levels: optically driven evolution in a biexciton system

The quantum control of a two-level system formed by the ground state and a single exciton exploits only small part of the possibilities offered by a QD. Much more interesting physics, as well as potential applications, becomes available if all the states are involved in the dynamics. Below we study two quantum optical schemes involving the confined biexciton system. First, the theory of the experimentally observed two-photon Rabi oscillations is given.¹⁸ Then, a theoretical proposal for an experiment highlighting the role of quantum complementarity in time-domain interference is described.²⁴

1.5.1. Two-photon Rabi oscillations

If we apply circularly polarized excitation to a QD in the ground state we can only create single excitons, as follows from the selection rules discussed in Sec. 1.2 and from the Pauli exclusion principle. By using linear polarization, which is a superposition of two equal σ_+ and σ_- polarized components, one enables also biexciton generation. In this case, the ground state is coupled to the biexciton state via both exciton states. Here we will consider a situation in which the laser frequency is tuned to the two-photon resonance with the biexciton, while the single-exciton states are detuned by $\Delta = E_B/2$, as shown in Fig. 1.2b.

In the rotating wave approximation, the Hamiltonian of the biexcitonic system described above can be written in the form

$$H = \frac{E_B}{2} (|+\rangle\langle+| + |-\rangle\langle-|) + \frac{f(t)}{2\sqrt{2}} [(|g\rangle + |XX\rangle)(\langle+| + \langle-|) + \text{H.c.}], \quad (1.12)$$

where $|+\rangle, |-\rangle$ and $|XX\rangle$ are the σ_+ , σ_- and biexciton states, respectively. Thus, the laser pulse couples only one (bright) combination of the states ground and biexciton states, $|B\rangle = (|g\rangle + |XX\rangle)/\sqrt{2}$ to one (π_x -polarized) single exciton state $|X\rangle = (|+\rangle + |-\rangle)/\sqrt{2}$.

The system evolution is easily described in the new basis $|Y\rangle = (|+\rangle - |-\rangle)/\sqrt{2}, |D\rangle = (|g\rangle - |XX\rangle)/\sqrt{2}, |X\rangle, |B\rangle$, where the first two states are the (decoupled) π_y -polarized exciton state and the dark combination of the states ground and biexciton states. In this basis, the Hamiltonian (1.12) can be written as

$$H = \begin{pmatrix} E_B/2 & 0 & 0 & 0 \\ 0 & 0 & 0 & 0 \\ 0 & 0 & E_B/2 & f(t)/\sqrt{2} \\ 0 & 0 & f(t)/\sqrt{2} & 0 \end{pmatrix}, \quad (1.13)$$

which corresponds to the detuned rotation in the invariant subspace spanned by the x -polarized exciton state $|X\rangle$ and the state $|B\rangle$, while the first two states are decoupled and undergo only a trivial evolution. The initial (ground) state is now written as $|g\rangle = \frac{|D\rangle + |B\rangle}{\sqrt{2}}$.

Let us consider the instantaneous (for fixed t) eigenstates of the Hamiltonian (1.13) as a function of $f(t)$. For a large binding energy E_B the two branches belonging to the non-trivial two-dimensional invariant subspace are always widely separated. Thus, under the action of a sufficiently slowly varying laser pulse the system undergoes an adiabatic evolution with the pulse envelope $f(t)$ playing the role of a slowly varying parameter of the

Hamiltonian. Therefore, one can assume³⁰ that at each time t the state corresponds to the adiabatic (instantaneous) eigenstate of the Hamiltonian (1.13), i.e.,

$$|\psi(t)\rangle = \frac{|D\rangle + [c_-(t)|X\rangle + c_+(t)|B\rangle] e^{-i\Lambda(t)}}{\sqrt{2}},$$

where

$$c_{\pm}(t) = \frac{1}{\sqrt{2}} \left(1 \pm \frac{E_B}{\sqrt{(E_B)^2 + 8f^2(t)}} \right)^{1/2},$$

and

$$\Lambda(t) = \frac{1}{4\hbar} \int_{-\infty}^t d\tau \left(E_B - \sqrt{(E_B)^2 + 8f^2(\tau)} \right). \quad (1.14)$$

After the laser pulse has been switched off, the state becomes

$$|\psi\rangle = \frac{|D\rangle + e^{-i\Lambda(\infty)}|B\rangle}{\sqrt{2}} = e^{-i\Lambda(\infty)/2} \left(\cos \frac{\Lambda(\infty)}{2} |g\rangle + \sin \frac{\Lambda(\infty)}{2} |XX\rangle \right). \quad (1.15)$$

and coincides with the biexciton state for $\Lambda(\infty) = \pi$. Thus, the system effectively performs Rabi oscillations between the ground state and the biexciton state, with the occupation of the biexciton state given by

$$N_{XX} = |\langle XX|\psi\rangle|^2 = \sin^2 \frac{\Lambda(\infty)}{2}. \quad (1.16)$$

For $\theta \ll \tau_0 \Delta E_B / \hbar$ one has

$$\Lambda(\infty) \approx \frac{1}{\hbar \Delta E_B} \int_{-\infty}^{\infty} dt f^2(t) = \frac{4\hbar \text{Arcosh} \sqrt{2}}{\pi^2 \Delta E_B \tau_0} \theta^2$$

and the biexciton occupation N_{XX} grows as θ^4 , i.e., proportional to the square of the pulse intensity, as expected for a two-photon process (see Fig. 1.3).

It should be noted that the pulse area appearing as the parameter of the standard Rabi oscillations is now replaced by the adiabatic dynamical phase Λ , which is a nontrivial functional of the pulse shape [Eq. (1.14)]. In this way, the simple universal dynamics of a resonantly driven two level system, described by the area theorem, is replaced by a more complicated pattern of oscillations, depending on the detuning parameter $\tau_p E_B$ but also on the exact pulse shape (e.g. Gaussian vs. sech^{18}). The absence of any single exciton occupation in the final state is obviously due to the fact that the adiabatic limit corresponds to weak and long (i.e., spectrally narrow) pulses

and the excitation of single-exciton states becomes forbidden by energy conservation. Nonetheless, during the evolution the single-exciton states are also occupied.

1.5.2. *Quantum complementarity in time-domain interference experiments*

This Section discusses the essential modification to time domain interference experiments (Sec. 1.4.3) that allows one to attain partial information on the state of the system and to observe the related visibility reduction of the interference pattern. First, however, a measure of the partial information is introduced and the complementarity principle is formulated in a quantitative form.^{31,32}

The notion of “partial information” is understood as follows. The system (S) of interest is coupled to another *quantum probe* (QP) system and conditional dynamics of the latter is induced, leading to correlations between the states of the systems S and QP. Next, a measurement on QP is performed and its result is used to infer the state of S, i.e., to predict the outcome of a subsequent measurement on S. The probability of a correct prediction ranges from 1/2 (guessing at random in absence of any correlations) to 1 (knowing for sure, when the systems are maximally entangled).

Quantitatively, an intrinsic measure of information on the system S extracted by QP is provided by the *distinguishability of states*,^{31,32}

$$\mathcal{D} = 2 \left(p - \frac{1}{2} \right), \quad (1.17)$$

where p is the probability a correct prediction for the state of S maximized over all possible measurements on QP. In this way, guessing at random and knowing for sure correspond to $\mathcal{D} = 0$ and $\mathcal{D} = 1$, respectively. According to a general theory,^{31,32} the complementarity relation between the knowledge of the system state and the visibility of the fringes may be written, using the distinguishability \mathcal{D} as a measure of information, in the quantitative form,

$$\mathcal{D}^2 + \mathcal{V}^2 \leq 1. \quad (1.18)$$

The equality holds for systems in pure states.

In a QD, this formal scheme translates naturally into the conditional dynamics of a biexcitonic system (Fig.1.2a), as described in Sec. 1.3. Thus, the exciton addressed in the interference experiment described in Sec. 1.4.3

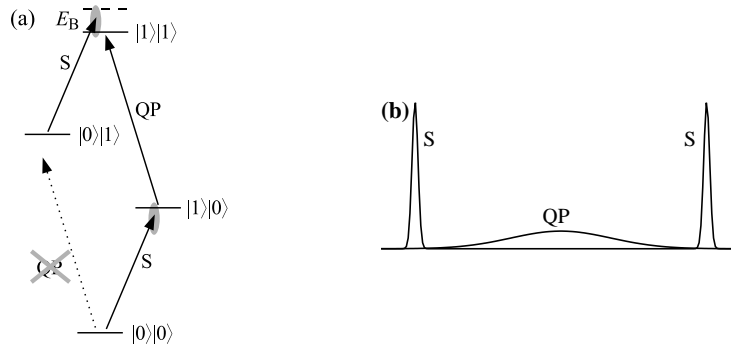


Fig. 1.6. (a) The diagram of energy levels and transitions in the system, assuming that the excitons are confined in neighboring dots with different transition energies. The pulses inducing transitions on the system S have broad spectrum so that both transitions are possible. The pulse acting on the QP system is spectrally selective and tuned to the biexcitonic transition, so that the single-exciton transition is energetically forbidden in this subsystem. (b) The sequence of pulses used in the experiment.

is, say, the σ_+ exciton (system S). The other degree of freedom of the biexciton system (the σ_- exciton) will be used as the quantum probe.

We will use a tensor product notation with $|0\rangle$ and $|1\rangle$ denoting the absence and presence of the respective exciton, as previously, with the interfering system (S) always to the left. In the rotating basis with respect to both subsystems, the RWA Hamiltonian for the biexciton system is

$$H = H_1 \otimes \mathbb{I} + \Delta|1\rangle\langle 1| \otimes |1\rangle\langle 1| + \frac{1}{2}f_{\text{QP}}(t - \tau_{\text{QP}})\mathbb{I} \otimes (|0\rangle\langle 1| + \text{H.c.}) \quad (1.19)$$

where Δ is the bi-exciton energy shift and $E_{\text{QP}}(t)$ is the envelope of the pulse coupled to the QP exciton. Here the first term denotes the Hamiltonian (1.9) and corresponds to the pulse sequence of the interference experiment described in Sec. 1.4.3, the second one accounts for the bi-excitonic energy shift and the third term describes the action of the pulse coupled to the second (QP) exciton and spectrally tuned to the exciton-biexciton transition. This pulse arrives at $t = \tau_{\text{QP}}$, between the other two pulses (that is, $0 < t_{\text{QP}} < \tau$), and will induce the conditional dynamics. Its phase is irrelevant and will be assumed 0. The structure of system excitations and the sequence of pulses are shown in Fig. 1.6.

Assume that the exciton (system S) is in the equal superposition state (1.10). The probability of correctly guessing the result of a measurement in the $|0\rangle, |1\rangle$ basis without any additional information is obviously $1/2$. Now, we can correlate this excitonic system with the other one (QP; initially in

the state $|0\rangle$). To this end, one applies a selective (spectrally narrow) pulse with the area α (the arrow labelled ‘QP’ in Fig. 1.6a). This rotates the state of the second subsystem according to Eq. (1.6) (with $\hat{\mathbf{n}} = [1, 0, 0]$) if and only if the first system is in the state $|1\rangle$. The corresponding unitary transformation of the compound system is

$$U_{\text{QP}} = |0\rangle\langle 0| \otimes \mathbb{I} + |1\rangle\langle 1| \otimes \left(\cos \frac{\alpha}{2} \mathbb{I} - i \sin \frac{\alpha}{2} \sigma_x \right),$$

and takes the state $|\psi\rangle$ into

$$|\psi'\rangle = \frac{1}{\sqrt{2}}|0\rangle \otimes |0\rangle - \frac{i}{\sqrt{2}}|1\rangle \otimes \left(\cos \frac{\alpha}{2}|0\rangle - i \sin \frac{\alpha}{2}|1\rangle \right).$$

For $\alpha = \pi$, this pulse performs a CNOT-like transformation²⁶ on the biexcitonic system. As a result, the total system is in the maximally entangled state $(|0\rangle|0\rangle - i|1\rangle|1\rangle)/2$ and a measurement on the QP system uniquely determines the state of the system S. Hence, due to quantum correlations between the systems, complete information on the state of S has been extracted to QP. On the other hand, if the biexciton is excited with a pulse with area $\alpha < \pi$ the correlation between the subsystems is weaker and a measurement on QP cannot fully determine the state of S, although the attained information may increase the probability for correctly predicting the result of a subsequent measurement on S. According to the discussion above, this means that partial information on the state of S is available.

In order to find the distinguishability measure in the biexciton scheme discussed here, we write the density matrix of the total system corresponding to the state $|\psi'\rangle$,

$$\varrho = \frac{1}{2} \sum_{nm} |n\rangle\langle m| \otimes \rho_{nm}, \quad (1.20)$$

with $\rho_{00} = |0\rangle\langle 0|$, $\rho_{11} = \frac{1}{2}(\mathbb{I} + \cos \alpha \sigma_z - \sin \alpha \sigma_y)$, $\rho_{01} = \rho_{10}^\dagger = i \cos \frac{\alpha}{2}|0\rangle\langle 0| - \sin \frac{\alpha}{2}|0\rangle\langle 1|$. Note that ρ_{00} and ρ_{11} (but not ρ_{01}) are density matrices.

According to the general theory,^{31,32} the best chance for correctly guessing the state of S results from the measurement of the observable $\rho_{00} - \rho_{11}$ and the probability of the correct prediction is then $p = \frac{1}{2} + \frac{1}{4} \text{Tr} |\rho_{00} - \rho_{11}|$ where $|\rho|$ is the modulus of the operator ρ . Using the explicit forms of the density matrices ρ_{00}, ρ_{11} and the definition (1.17) one finds for the distinguishability in our case

$$\mathcal{D} = \frac{1}{2} \text{Tr} |\rho_{00} - \rho_{11}| = \left| \sin \frac{\alpha}{2} \right|. \quad (1.21)$$

Thus, the amount of information on the system S accessible via a measurement on QP increases from 0 (no QP pulse at all) to 1 (for a π pulse).

Next, we study the effect of extracting the which path information on the interference fringes. In the state (1.20), the reduced density matrix of the subsystem S is $\rho_S = \text{Tr}_{\text{QP}} \rho = (1/2)(\mathbb{I} - \cos(\alpha/2)\sigma_y)$. Upon applying the second pulse of the interference experiment scheme, namely the unconditional $\pi/2$ pulse [Eq. (1.11)], the average number of excitons in the dot is

$$N(\phi) = \langle 1 | U_2 \rho_S U_2^\dagger | 1 \rangle = \frac{1}{2} \left(1 - \cos \frac{\alpha}{2} \cos \phi \right).$$

Now, the average occupation oscillates between the limiting values $(1 \pm |\cos \alpha|)/2$ and the visibility of the fringes is

$$\mathcal{V} = |\cos(\alpha/2)|. \quad (1.22)$$

Comparing Eq. (1.22) with Eq. (1.21) it is clear that the more certain one is whether the exciton *is there* or *not* (\mathcal{D} increases), the less clear the interference fringes become (\mathcal{V} decreases). Quantitatively, the relation $\mathcal{D}^2 + \mathcal{V}^2 = 1$ holds which is consistent with the complementarity relation (1.18). It can be shown that, in the presence of coupling to the environment, where both subsystems are in mixed states due to dephasing, this relation will turn into inequality.²⁴ Let us notice that the impact of the which path information on interference fringes is the same no matter whether the QP subsystem is measured before or after generating and detecting the interference fringes and even whether it is measured at all.

The time-domain manifestation of quantum complementarity discussed here not only broadens the class of experiments in which fundamental aspects of the quantum world may be tested but also has the advantage of being independent of the position-momentum (Heisenberg's) uncertainty that has been historically tied to the space-domain discussions of complementarity.³³ In fact, it is independent of any uncertainty principles whatsoever. Indeed, the only two quantities which are measured in the time-domain interference experiment are the occupations of two different excitons. These quantities refer to *different subsystems* and, therefore, are obviously *commuting* and simultaneously measurable. Although the quantum probe exciton is created in a way that correlates it with the presence of the other exciton (S), this cannot be interpreted as a (projective) measurement on S, since the QP exciton is definitely a quantum (microscopic) system and not a classical, macroscopic measurement device. Thus, the experimental procedure described in this section demonstrates quantum

complementarity in its pure form, involving only the notion of *information* on the system state and independent of any uncertainty relations between non-commuting observables.

Further discussion of the concept of complementarity in the context of optical experiments on QDs, including the analysis of its feasibility in terms of the currently available experimental techniques and of the parameters of the existing structures, as well as the analysis of the role of dephasing is given in Ref. 24.

1.6. Carrier-phonon interaction in quantum dots

This section presents the derivation of the coupling constants between bulk phonon modes and confined carriers in a semiconductor.^{34,35} We will restrict ourselves to the deformation potential coupling, which is relevant for the discussion in the following sections. The treatment of other couplings (piezoelectric and polar) is reviewed in Ref. 36.

Any crystal deformation leads to shifts of the conduction (c) and valence (v) bands which are, to the leading order, proportional to the relative volume change. The corresponding contribution to the energy of electrons (e) and holes (h) in the long-wavelength limit is

$$H_{e/h}^{(\text{DP})} \equiv \pm \Delta E_{c/v} = \mp \sigma_{e/h} \frac{\delta V}{V},$$

where $\sigma_{e/h}$ are the deformation potential constants for electrons and holes and V is the unit cell volume. Using the strain tensor $\hat{\sigma}$,

$$\sigma_{ij} = \frac{1}{2} \left(\frac{\partial u_i}{\partial r_j} + \frac{\partial u_j}{\partial r_i} \right),$$

one may write $H_{e/h}^{(\text{DP})} = \mp \sigma_{e/h} \text{Tr} \hat{\sigma} = \mp \sigma_{e/h} \nabla \cdot \mathbf{u}(\mathbf{r})$, where $\mathbf{u}(\mathbf{r})$ is the local displacement field. The displacement is quantized in terms of phonons,

$$\mathbf{u}(\mathbf{r}) = i \frac{1}{\sqrt{N}} \sum_{\mathbf{k}} \sqrt{\frac{\hbar}{2\rho V \omega_{\mathbf{k}}}} \hat{\mathbf{e}}_{\mathbf{k}} (b_{\mathbf{k}} + b_{-\mathbf{k}}^\dagger) e^{i\mathbf{k} \cdot \mathbf{r}}, \quad (1.23)$$

where $\omega_{\mathbf{k}}$ is the frequency for the wave vector \mathbf{k} , $\hat{\mathbf{e}}_{\mathbf{k}} = -\hat{\mathbf{e}}_{-\mathbf{k}}$ is the corresponding real unit polarization vector, and ρ is the crystal density. Only the longitudinal branch contributes to $\nabla \cdot \mathbf{u}$ in (1.23) and the final interaction Hamiltonian in the coordinate representation for carriers is

$$H_{e/h}^{(\text{DP})} = \pm \sigma_{e/h} \frac{1}{\sqrt{N}} \sum_{\mathbf{k}} \sqrt{\frac{\hbar k}{2\rho V \omega_{\mathbf{k}}}} (b_{\mathbf{k}} + b_{-\mathbf{k}}^\dagger) e^{i\mathbf{k} \cdot \mathbf{r}}. \quad (1.24)$$

In the second quantization representation with respect to the carrier states this reads

$$\begin{aligned} H_{e/h}^{(\text{DP})} &= \sum_{nn'} \langle n|V(\mathbf{r})|n'\rangle a_n^\dagger a_{n'} = \sum_{nn'} \int_{-\infty}^{\infty} d^3r \psi_n^*(\mathbf{r}) V(\mathbf{r}) \psi_{n'}(\mathbf{r}) a_n^\dagger a_{n'} \\ &= \frac{1}{\sqrt{N}} \sum_{knn'} a_n^\dagger a_{n'} f_{e/h,nn'}^{(\text{DP})}(\mathbf{k}) (b_{\mathbf{k}} + b_{-\mathbf{k}}^\dagger), \end{aligned} \quad (1.25)$$

where $f_{e/h,nn'}^{(\text{DP})}(\mathbf{k}) = \sigma_{e/h} \sqrt{\frac{\hbar k}{2\rho V c}} \mathcal{F}_{nn'}(\mathbf{k})$, with the formfactor

$$\mathcal{F}_{nn'}(\mathbf{k}) = \int_{-\infty}^{\infty} d^3r \psi_n^*(\mathbf{r}) e^{i\mathbf{k}\cdot\mathbf{r}} \psi_{n'}(\mathbf{r}) = \mathcal{F}_{n'n}^*(-\mathbf{k}). \quad (1.26)$$

While the common coefficient of the coupling Hamiltonian contains the fundamental and material-dependent constants and reflects general electrical and mechanical properties of the semiconductor system, the formfactor (1.26) contains information about the geometry of the confinement and the resulting properties of wave functions. In this sense, it is the “engineerable” part of the carrier-phonon coupling.

From the orthogonality of single-particle states one immediately has $\mathcal{F}_{nn'}(0) = \delta_{nn'}$. If the wave functions are localized at a length l , then the extent of the formfactor is $\sim 1/l$. Thus, for carrier states localized in a QD over many lattice sites and smooth within this range, the functions $\mathcal{F}_{nn'}(\mathbf{k})$ will be localized in \mathbf{k} -space very close to the center of the Brillouin zone.

As an example, let us consider a Gaussian wave function,

$$\psi(\mathbf{r}) = \frac{1}{\pi^{3/4} l_\perp l_z} \exp \left[-\frac{1}{2} \left(\frac{r_\perp}{l_\perp} \right)^2 - \frac{1}{2} \left(\frac{z}{l_z} \right)^2 \right], \quad (1.27)$$

where r_\perp is the position component in the xy plane and l_\perp, l_z are the localization widths in-plane and in the growth (z) direction. The corresponding formfactor is then easily found to be

$$\mathcal{F}(\mathbf{k}) = \exp \left[-\left(\frac{k_\perp l_\perp}{2} \right)^2 - \frac{1}{2} \left(\frac{k_z l_z}{2} \right)^2 \right]. \quad (1.28)$$

The formulas derived above describe the interaction in the single-particle basis. However, most of the following deals with excitonic states, i.e. states of confined electron-hole pairs interacting by Coulomb potentials. Both carriers forming the exciton couple to phonons according to Eq. (1.25). For the further discussion in this chapter it is sufficient to discuss the lowest exciton state. It is reasonable to assume its wave function

approximately in a product form,³⁷ i.e.,

$$|1\rangle = a_{e,0}^\dagger a_{h,0}^\dagger |0\rangle,$$

where $a_{e/h,0}^\dagger$ create an electron and a hole in the ground confined state in the QD. Then, one gets from Eq. (1.25) the following coupling constant between the confined exciton and phonons for the deformation potential interaction

$$g_{\mathbf{k}} = \sqrt{\frac{\hbar k}{2\rho V c_1}} \left(\sigma_e \mathcal{F}^{(e)}(\mathbf{k}) - \sigma_h \mathcal{F}^{(h)}(\mathbf{k}) \right). \quad (1.29)$$

Note that, due to different deformation potential constants $\sigma_{e/h}$, this coupling does not vanish even if the electron and hole wave functions are the same, leading to identical single-particle formfactors.

Thus, the exciton (restricted to its ground state) driven by a laser field and interacting with LA phonons via the deformation potential coupling is described by the Hamiltonian

$$H = H_{\text{RWA}} + \sum_{\mathbf{k}} \hbar\omega_{\mathbf{k}} b_{\mathbf{k}}^\dagger b_{\mathbf{k}} + |1\rangle\langle 1| \sum_{\mathbf{k}} g_{\mathbf{k}} (b_{\mathbf{k}} + b_{-\mathbf{k}}^\dagger), \quad (1.30)$$

where the first term describes the carrier subsystem and is given by Eq. (1.5).

The Hamiltonian (1.30) is the basis for the microscopic modeling of dephasing effects in QDs. It turns out that this relatively simple model is very successful in reproducing the experimental data.^{38,39} Hence, it may serve as a reliable starting point for describing the evolution of the combined system of confined carriers and lattice modes.

1.7. Theoretical methods for carrier–phonon kinetics

In this section we will study a few theoretical methods that have proven to be useful for the description of the carrier-phonon quantum kinetics in QDs. This discussion will be limited to the simplest case of a two-level system described by the Hamiltonian (1.30).

1.7.1. *Exact solution for ultrafast excitations*

Let us start with the case of an ultrafast excitation. A very short laser pulse prepares the system in a certain superposition (dependent on the pulse phase and intensity) of the ground state $|0\rangle$ (no exciton) and the single-exciton state $|1\rangle$. By *very short* we mean a pulse much shorter than

the time scales of phonon dynamics, so that the preparation of the initial state may be considered instantaneous. This corresponds to the actual experimental situation with pulse durations of the order of 100 fs.⁴⁰ On the other hand, the pulse is long enough to assure a relatively narrow spectrum and to prevent the population of higher confined levels and excitation of optical phonons.⁴¹ In this ultrafast limit the only role of the laser pulse is to prepare the initial state, while the subsequent evolution is generated by a time-independent Hamiltonian,

$$H = -\Delta|1\rangle\langle 1| + \sum_{\mathbf{k}} \hbar\omega_{\mathbf{k}} b_{\mathbf{k}}^{\dagger} b_{\mathbf{k}} + |1\rangle\langle 1| \sum_{\mathbf{k}} g_{\mathbf{k}} (b_{\mathbf{k}} + b_{-\mathbf{k}}^{\dagger}), \quad (1.31)$$

obtained by setting $H_{\text{RWA}} = -\Delta|1\rangle\langle 1|$ in Eq. (1.30).

In a superposition state created by the laser pulse [Eq. (1.7)] the interband component of the electric dipole moment has a non-vanishing average value oscillating at an optical frequency (hence referred to as *optical polarization*)⁴² which leads to the emission of coherent electromagnetic radiation with an amplitude proportional to the oscillating dipole moment. In an unperturbed system (e.g., in an atom), the radiation would be emitted over time of the order of the lifetime of the superposition state, i.e., until the system relaxes to the ground state due to radiative energy loss.

In a semiconductor structure an additional effect, related to carrier-phonon coupling, appears on a time scale much shorter than the lifetime of the state. The last two terms in Eq. (1.31) describe a set of harmonic oscillators which, in the presence of the exciton, are displaced by an external force proportional to the coupling constant $g_{\mathbf{k}}$. This means that, due to the interactions between confined carriers and lattice ions, the ground state of the lattice in the presence of a charge distribution is different than in its absence. As a result, after the creation of a confined exciton the lattice relaxes to a new equilibrium, which is accompanied by the emission of phonon wave packets^{37,43} that form a trace in the macroscopic crystal distinguishing the exciton state from an empty dot. This information broadcast via emitted phonons leads to a decay of the coherence of the superposition state⁴⁴ although the average occupations of the system states remain unaffected (hence the process is referred to as *pure dephasing*). Since coherent dipole radiation requires well-defined phase relations between the components of a quantum superposition, the amplitude of this radiation, measured in the experiment, gives access to the coherence properties of the quantum state of confined carriers itself. The dephasing of the quantum superposition is therefore directly translated into the decay of coherent optical radiation

from the system.

As discussed in Sec. 1.6, the carrier-phonon interaction term in Eq. (1.31) is linear in phonon operators and describes a shift of the lattice equilibrium induced by the presence of a charge distribution in the dot. The stationary state of the system corresponds to the exciton and the surrounding coherent cloud of phonons representing the lattice distortion to the new equilibrium. The transformation that creates the coherent cloud is the shift $w b_{\mathbf{k}} w^\dagger = b_{\mathbf{k}} - f_{\mathbf{k}}/(\hbar\omega_{\mathbf{k}})$, generated by the Weyl operator^{35,44}

$$w = \exp \left[\sum_{\mathbf{k}} \left(\frac{g_{\mathbf{k}}^*}{\hbar\omega_{\mathbf{k}}} b_{\mathbf{k}}^\dagger - \frac{g_{\mathbf{k}}}{\hbar\omega_{\mathbf{k}}} b_{\mathbf{k}} \right) \right]. \quad (1.32)$$

A straightforward calculation shows that the Hamiltonian (1.31) is diagonalized by the unitary transformation $W = |0\rangle\langle 0| \otimes \mathbb{I} + |1\rangle\langle 1| \otimes w$, where \mathbb{I} is the identity operator and the tensor product refers to the carrier subsystem (first component) and its phonon environment (second component). As a result one gets

$$\tilde{H} = W H W^\dagger = -\tilde{\Delta} |1\rangle\langle 1| + H_{\text{ph}},$$

where $\tilde{\Delta} = \Delta + \sum_{\mathbf{k}} |g_{\mathbf{k}}|^2/(\hbar\omega_{\mathbf{k}})$ and $H_{\text{ph}} = \sum_{\mathbf{k}} \hbar\omega_{\mathbf{k}} b_{\mathbf{k}}^\dagger b_{\mathbf{k}}$.

We assume that at the beginning ($t = 0$) the state of the whole system is $\rho_0 = (|\Psi\rangle\langle\Psi|) \otimes \rho_{\text{ph}}$, where ρ_{ph} is the density matrix of the phonon subsystem (environment) at thermal equilibrium and $|\Psi\rangle$ is given by Eq. (1.7). For simplicity, we will assume an equal superposition state, setting $\alpha = \pi/2$ and $\varphi = -\pi/2$.

The evolution operator $U(t) = e^{-iHt/\hbar}$ may be written as

$$\begin{aligned} U(t) &= W^\dagger W U(t) W^\dagger W = W^\dagger \tilde{U}(t) W = W^\dagger \tilde{U}(t) W \tilde{U}^\dagger(t) \tilde{U}(t) \\ &= W^\dagger W(t) \tilde{U}(t), \end{aligned}$$

where $\tilde{U}(t) = e^{-i\tilde{H}t/\hbar}$ and $W(t) = \tilde{U}(t) W \tilde{U}^\dagger(t)$. Since $\tilde{U}(t)$ is diagonal the explicit form of $W(t)$ may easily be found and one gets

$$U(t) = [|0\rangle\langle 0| \otimes \mathbb{I} + |1\rangle\langle 1| \otimes w^\dagger w(t)] \tilde{U}(t), \quad (1.33)$$

where $w(t) = e^{-iH_{\text{ph}}t/\hbar} w e^{iH_{\text{ph}}t/\hbar}$.

Using the evolution operator in the form (1.33) the system state at a time t may be written as

$$\rho(t) = \frac{1}{2} \begin{pmatrix} \rho_{\text{E}} & e^{-i\tilde{\Delta}t/\hbar} \rho_{\text{E}} w^\dagger(t) w \\ e^{i\tilde{\Delta}t/\hbar} w^\dagger w(t) \rho_{\text{ph}} & w^\dagger w(t) \rho_{\text{ph}} w^\dagger(t) w \end{pmatrix}, \quad (1.34)$$

where we used the tensor product notation in which an operator A is expanded as $A = \sum_{m,n} |m\rangle\langle n| \otimes A_{mn}$ with a set of operators A_{mn} acting on the second subsystem, and written in the matrix form with respect to the first subsystem. The density matrix for the carrier subsystem is obtained by tracing out the phonon degrees of freedom, i.e., $\rho_S = \text{Tr}_E \rho$. Hence,

$$\rho_S(t) = \frac{1}{2} \begin{pmatrix} 1 & e^{-i\tilde{\Delta}t/\hbar} \langle w^\dagger(t)w \rangle \\ e^{i\tilde{\Delta}t/\hbar} \langle w^\dagger w(t) \rangle & 1 \end{pmatrix}. \quad (1.35)$$

The average may be calculated using two rules for Weyl operators.^{34,44} The multiplication of two operators of the form

$$w_i = \exp \left[\sum_{\mathbf{k}} \left(g_{\mathbf{k}}^{(i)*} \gamma_{\mathbf{k}}^\dagger - \gamma_{\mathbf{k}}^{(i)} b_{\mathbf{k}} \right) \right], \quad i = 1, 2, 3 \quad (1.36)$$

yields

$$w_1 w_2 = w_3 \exp \left[\frac{1}{2} \sum_{\mathbf{k}} \left(\gamma_{\mathbf{k}}^{(1)*} \gamma_{\mathbf{k}}^{(2)} - \gamma_{\mathbf{k}}^{(1)} \gamma_{\mathbf{k}}^{(2)*} \right) \right], \quad (1.37)$$

where w_3 is given by Eq. (1.36) with $\gamma_{\mathbf{k}}^{(3)} = \gamma_{\mathbf{k}}^{(1)} + \gamma_{\mathbf{k}}^{(2)}$. The rule for averaging of an operator given by Eq. (1.36) in the thermal equilibrium state is

$$\langle w_i \rangle = e^{-\frac{1}{2} \sum_{\mathbf{k}} |\gamma_{\mathbf{k}}^{(i)}|^2 (2n_{\mathbf{k}} + 1)}, \quad (1.38)$$

where $n_{\mathbf{k}}$ are bosonic equilibrium occupation numbers. The final result is

$$\langle w^\dagger(t)w \rangle = \exp \left\{ - \sum_{\mathbf{k}} \left| \frac{g_{\mathbf{k}}}{\hbar\omega_{\mathbf{k}}} \right|^2 [i \sin \omega_{\mathbf{k}} t + (1 - \cos \omega_{\mathbf{k}} t)(2n_{\mathbf{k}} + 1)] \right\}.$$

The emitted coherent dipole radiation is proportional to the non-diagonal element of the density matrix $\rho_S(t)$ and its amplitude is

$$P(t) = P_0 |\langle w^\dagger(t)w \rangle|. \quad (1.39)$$

In Fig. 1.7 we show the normalized polarization amplitude $P(t)/P_0$ (originally derived in Ref. 45). The interaction with the macroscopic crystal environment leads to a reduction of coherent radiation due to pure dephasing of the exciton state, reflected by the reduced value of the non-diagonal element of the density matrix ρ_S . At $t = 0$ one has $\langle w^\dagger(t)w \rangle = 1$, while at large values of t , $\cos \omega_{\mathbf{k}} t$ oscillates very quickly as a function of \mathbf{k} and

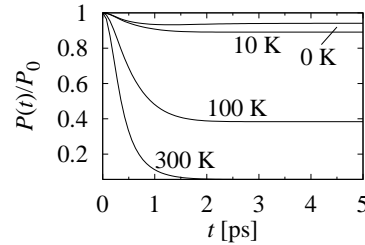


Fig. 1.7. Decay of the coherent radiation from a confined exciton at various temperatures, as shown. In our calculations we use typical parameters for a self-assembled InAs/GaAs structure: single particle wave functions $\psi(\mathbf{r})$ modelled by Gaussians with $l_{\perp} = 4$ nm and $l_z = 1$ nm [Eq.(1.27)], the deformation potential difference $\sigma_e - \sigma_h = 9.5$ eV, crystal density $\varrho = 5300$ kg/m³, and the speed of sound $c = 5150$ m/s.

averages to 0 (see also Ref. 45). Thus, for long times, the polarization amplitude tends to a temperature-dependent finite value

$$P(t) \rightarrow P_0 \exp \left[- \sum_{\mathbf{k}} \left| \frac{g_{\mathbf{k}}}{\hbar\omega_{\mathbf{k}}} \right|^2 (2n_{\mathbf{k}} + 1) \right] < P_0.$$

This partial decay of coherence is a characteristic feature of short-time dephasing for carrier-phonon couplings encountered in real systems.⁴⁰

1.7.2. Perturbation theory for driven systems

In this section we derive the equations for the reduced density matrix of the carrier subsystem to the leading order in the phonon coupling, assuming that the unperturbed evolution is known. This approach yields very simple and intuitive formulas that may easily be applied to a range of problems. Here, we will again restrict the formalism to a single exciton level. A more general discussion is given in Ref. 36.

As already mentioned, the evolution of the carrier subsystem is generated by the (time dependent) Hamiltonian H_{RWA} [Eq. (1.5)], describing the properties of the system itself as well as its coupling to driving fields. The evolution of the phonon subsystem (reservoir) is described by the Hamiltonian H_{ph} [the second term in Eq. (1.30)]. The evolution operator for the driven carrier subsystem and free phonon modes, without the carrier-phonon interaction, is

$$U_0(t) = U_{\text{RWA}}(t) \otimes e^{-iH_{\text{ph}}(t-s)},$$

where $U_{\text{RWA}}(t)$ is the operator for the unperturbed evolution of the carrier subsystem and s is the initial time.

The carrier-phonon coupling may be written in the form $V = S \otimes R$, where S acts in the Hilbert space of the carrier subsystem while the time-independent R affect only the environment. For instance, in the special case of Eq. (1.30), $S = |1\rangle\langle 1|$ and

$$R = \frac{1}{\sqrt{N}} \sum_{\mathbf{k}} g_{\mathbf{k}} (b_{\mathbf{k}} + b_{-\mathbf{k}}^{\dagger}). \quad (1.40)$$

We will assume that at the initial time s the system is in the product state $\varrho(s) = |\psi_0\rangle\langle\psi_0| \otimes \rho_{\text{ph}}$, where $|\psi_0\rangle$ is a certain state of the carrier subsystem and ρ_{ph} is the thermal equilibrium distribution of phonon modes. Physically, such an assumption is usually reasonable due to the existence of two distinct time scales: the long one for the carrier decoherence (e.g. 1 ns ground state exciton lifetime^{40,46}) and the short one for the reservoir relaxation (1 ps dressing time^{37,40,45}).

The starting point is the evolution equation for the density matrix of the total system in the interaction picture with respect to the externally driven evolution U_0 , in the second order Born approximation with respect to the carrier-phonon interaction⁴⁷

$$\tilde{\varrho}(t) = \tilde{\varrho}(s) + \frac{1}{i\hbar} \int_s^t d\tau [V(\tau), \varrho(s)] - \frac{1}{\hbar^2} \int_s^t d\tau \int_s^{\tau} d\tau' [V(\tau), [V(\tau'), \varrho(s)]], \quad (1.41)$$

where $\tilde{\varrho}(t) = U_0^{\dagger}(t)\varrho(t)U_0(t)$, $V(t) = U_0^{\dagger}(t)VU_0(t)$ (it should be kept in mind that, in general, V may depend on time itself).

The reduced density matrix of the carrier subsystem at time t is $\rho(t) = U_{\text{RWA}}(t)\tilde{\rho}(t)U_{\text{RWA}}^{\dagger}(t)$, $\tilde{\rho}(t) = \text{Tr}_{\text{R}}\tilde{\varrho}(t)$, where the trace is taken over the phonon degrees of freedom. The first (zeroth order) term in (1.41) gives

$$\rho^{(0)}(t) = U_{\text{RWA}}(t)|\psi_0\rangle\langle\psi_0|U_{\text{RWA}}^{\dagger}(t) = |\psi_0(t)\rangle\langle\psi_0(t)|. \quad (1.42)$$

The second term vanishes, since it contains the thermal average of an odd number of phonon operators. The third (second order) term describes the leading phonon correction to the dynamics of the carrier subsystem,

$$\tilde{\rho}^{(2)}(t) = -\frac{1}{\hbar^2} \int_s^t d\tau \int_s^{\tau} d\tau' \text{Tr}_{\text{R}}[V(\tau), [V(\tau'), \varrho(s)]]. \quad (1.43)$$

First of the four terms resulting from expanding the commutators in (1.43) is (I) = $-Q_t|\psi_0\rangle\langle\psi_0|$, where

$$Q_t = \frac{1}{\hbar^2} \int_s^t d\tau \int_s^{\tau} d\tau' S(\tau)S(\tau')\langle R(\tau - \tau')R \rangle. \quad (1.44)$$

The operators S and R are transformed into the interaction picture in the usual way $S(t) = U_0^\dagger(t)SU_0(t)$, $R(t) = U_0^\dagger(t)RU_0(t)$ and $\langle \hat{O} \rangle = \text{Tr}_R[\hat{O}\rho_{\text{ph}}]$ denotes the thermal average (obviously $[U_0(t), \rho_{\text{ph}}] = 0$).

The second term is

$$(II) = \frac{1}{\hbar^2} \int_s^t d\tau \int_s^\tau d\tau' |\psi_0\rangle\langle\psi_0| S(\tau') S(\tau) \langle R(\tau' - \tau) R \rangle = -|\psi_0\rangle\langle\psi_0| Q_t^\dagger,$$

where we used the relation $\langle R(\tau' - \tau) R \rangle = \langle R(\tau - \tau') R \rangle^*$.

In a similar manner, the two other terms may be combined into

$$(III) + (IV) = \hat{\Phi}_t [|\psi_0\rangle\langle\psi_0|].$$

where

$$\hat{\Phi}_t [\rho] = \frac{1}{\hbar^2} \int_s^t d\tau \int_s^\tau d\tau' S(\tau') \rho S(\tau) \langle R(\tau - \tau') R \rangle. \quad (1.45)$$

In terms of the new Hermitian operators

$$A_t = Q_t + Q_t^\dagger, \quad h_t = \frac{1}{2i}(Q_t - Q_t^\dagger), \quad (1.46)$$

the density matrix at the final time t (1.42,1.43) may be written as

$$\rho(t) = U_{\text{RWA}}(t) \left(|\psi_0\rangle\langle\psi_0| - i [h_t, |\psi_0\rangle\langle\psi_0|] - \frac{1}{2} \{A_t, |\psi_0\rangle\langle\psi_0|\} + \hat{\Phi}_t [|\psi_0\rangle\langle\psi_0|] \right) U_{\text{RWA}}^\dagger. \quad (1.47)$$

The first term is a Hamiltonian correction which does not lead to irreversible effects and, in principle, may be compensated by an appropriate modification of the control Hamiltonian H_{RWA} . The other two terms describe processes of entangling the system with the reservoir, leading to the loss of coherence of the carrier state.

Let us introduce the spectral density of the reservoir,

$$R(\omega) = \frac{1}{2\pi\hbar^2} \int dt \langle R(t) R \rangle e^{i\omega t}. \quad (1.48)$$

For the operators given in Eq. (1.40) one has explicitly

$$R(\omega) = \frac{1}{\hbar^2} |n_{\text{B}}(\omega) + 1| \frac{1}{N} \sum_{\mathbf{k}} |g_{\mathbf{k}}|^2 [\delta(\omega - \omega_{\mathbf{k}}) + \delta(\omega + \omega_{\mathbf{k}})], \quad (1.49)$$

where $n_{\text{B}}(\omega) = -n_{\text{B}}(-\omega) - 1$ is the Bose distribution function. The spectral density $R(\omega)$ depends on the material parameters and system geometry

and characterizes the properties of the lattice subsystem. For the deformation potential coupling to LA phonons, it has the long-wavelength behavior $R(\omega) \sim \omega^3[n_B(\omega) + 1]$.

With the help of (1.48) one may write

$$\hat{\Phi}_t[\rho] = \int d\omega R(\omega) Y(\omega) \rho Y^\dagger(\omega) \quad (1.50)$$

where the frequency-dependent operators have been introduced,

$$Y(\omega) = \int_s^t d\tau S(\tau) e^{i\omega\tau}. \quad (1.51)$$

Using (1.48) again one has

$$Q_t = \int d\omega \int_s^t d\tau \int_s^t d\tau' \theta(\tau - \tau') S(\tau) S(\tau') R(\omega) e^{-i\omega(\tau - \tau')}.$$

Next, representing the Heaviside function as

$$\theta(t) = -e^{i\omega t} \int \frac{d\omega'}{2\pi i} \frac{e^{-i\omega' t}}{\omega' - \omega + i0^+},$$

we write

$$\begin{aligned} Q_t &= - \int d\omega R(\omega) \int \frac{d\omega'}{2\pi i} \frac{Y^\dagger(\omega') Y(\omega')}{\omega' - \omega + i0^+} \\ &= - \int d\omega R(\omega) \int \frac{d\omega'}{2\pi i} Y^\dagger(\omega') Y(\omega') \left[-i\pi\delta(\omega' - \omega) + \mathcal{P} \frac{1}{\omega' - \omega} \right], \end{aligned}$$

where \mathcal{P} denotes the principal value.

Hence, the two Hermitian operators defined in (1.46) take the form

$$A_t = \int d\omega R(\omega) Y^\dagger(\omega) Y(\omega) \quad (1.52)$$

and

$$h_t = \int d\omega R(\omega) \mathcal{P} \int \frac{d\omega'}{2\pi} \frac{Y^\dagger(\omega') Y(\omega')}{\omega' - \omega}. \quad (1.53)$$

In order to provide an example of an application of the perturbative method presented in this section let us consider a $\pi/2$ rotation of an excitonic two-level system in the presence of carrier-phonon coupling. As we have already pointed out, any fast change of the state of the carrier subsystem leads to spontaneous processes of lattice relaxation that affect the coherence of the carrier state. It is reasonable to expect that coherent control is recovered if the evolution of the carrier subsystem is slow (adiabatic) compared to the typical timescales of the lattice dynamics. Thus,

the requirement to avoid traces of carrier dynamics in the outside world favors slow operation on the carrier subsystem, contrary to other decoherence processes (of Markovian character), like radiative decay of the exciton or thermally activated processes of phonon-assisted transitions to higher states. The latter have the character of an exponential decay and, for short times, contribute an error $\tilde{\delta} = \tau_g/\tau_d$, where τ_g is the gating time and τ_d is the decay time constant. Here we consider the interplay between these two contributions to the error for the solid-state qubit implementation using excitonic (charge) states in quantum dots (QDs),⁴⁸ with computational states defined by the absence ($|0\rangle$) or presence ($|1\rangle$) of one exciton in the ground state of the dot, operated by resonant coupling to laser light. We show that it leads to a trade-off situation with a specific gating time corresponding to the minimum decoherence for a given operation.⁴⁹

To quantify the quality of the rotation, we use the *fidelity*²⁶

$$F = \langle \psi_0 | U_{\text{RWA}}^\dagger(\infty) \rho(\infty) U_{\text{RWA}}(\infty) | \psi_0 \rangle^{1/2} \quad (1.54)$$

which is a measure of the overlap between the ideal (pure) final state without perturbation, $U_{\text{RWA}}(\infty)\psi_0$, and the actual final state of the system given by the density matrix $\rho(\infty)$. If the procedure is performed ideally, i.e. without discrepancies from the desired qubit operation, then $F = 1$. The fidelity loss $\delta = 1 - F^2$ is referred to as the *error* of the quantum gate. Using the definition (1.54) and the Master equation (1.47), the error may be written in a general case as

$$\delta = \langle \psi_0 | A_t | \psi_0 \rangle - \left\langle \psi_0 \left| \hat{\Phi} [|\psi_0\rangle\langle\psi_0|] \right| \psi_0 \right\rangle.$$

It should be noted that the unitary correction generated by h_t does not contribute to the error at this order. Using the definitions (1.45,1.52) this may be further transformed into

$$\delta = \int d\omega R(\omega) |\langle \psi_\perp | Y(\omega) | \psi_0 \rangle|^2, \quad (1.55)$$

where ψ_\perp is a state orthogonal to $|\psi_0\rangle$ in the two-dimensional space of interest.

Since the coherence of superpositions induced by short pulses is unstable due to phonon-induced pure dephasing (Sec. 1.7.1), it seems reasonable to perform operations on *dressed states*, i.e. on the correctly defined quasiparticles of the interacting carrier-phonon system.⁵⁰ This may be formally achieved by employing the solid-state-theory concept of adiabatic switching on/off the interaction⁵¹ (as done in Ref. 52) to transform the states of

the noninteracting system into the states of the interacting one. Thus, we assume adiabatic switching on/off of the interaction with phonons by appending the appropriate exponent to the original interaction Hamiltonian [Eq. (1.30)],

$$H_{\text{int}} = e^{-\varepsilon|t|} \left[|1\rangle\langle 1| \sum_{\mathbf{k}} g_{\mathbf{k}} (b_{\mathbf{k}} + b_{-\mathbf{k}}^{\dagger}) \right], \quad (1.56)$$

where $\varepsilon = 0^+$. The operator S now becomes

$$S(t) = U_{\text{RWA}}(t) e^{-\varepsilon|t|} |1\rangle\langle 1| U_{\text{RWA}}^{\dagger}(t),$$

where the free evolution operator is generated by an optical pulse at the resonance (Sec. 1.4.2). The general formula (1.55) may now be used with the bare initial state $|\psi_0\rangle$. The adiabatic procedure assures that it is transformed to the dressed state before comparing it to the density matrix ρ , so that the fidelity is defined with respect to stable, dressed states.

The operator $Y(\omega)$ can be written in the form

$$\begin{aligned} Y(\omega) &= \frac{1}{4i\omega} F(\omega) (|1\rangle\langle 0| - |0\rangle\langle 1| + |0\rangle\langle 0| - |1\rangle\langle 1|) \\ &\quad + \frac{1}{4i\omega} F^*(-\omega) (|0\rangle\langle 1| - |1\rangle\langle 0| + |0\rangle\langle 0| - |1\rangle\langle 1|), \end{aligned}$$

where

$$F(\omega) = \int_{-\infty}^{\infty} d\tau e^{i\omega\tau} \frac{d}{d\tau} e^{i\Phi(\tau)}.$$

Since in quantum information processing applications the initial state of the quantum bit is in general not known, it is reasonable to consider the error averaged over all input states. Let us introduce the function

$$S(\omega) = \omega^2 |\langle \psi_{\perp} | Y(\omega) | \psi_0 \rangle|_{\text{av}}^2,$$

where the average is taken over the Bloch sphere. According to Eq. (1.55), the average error may now be written as

$$\delta = \int \frac{d\omega}{\omega^2} R(\omega) S(\omega). \quad (1.57)$$

The averaging is most conveniently performed by noting that

$$Y(\omega) = \frac{1}{2i\omega} F(\omega) |+\rangle\langle -| + \frac{1}{2i\omega} F^*(-\omega) |-\rangle\langle +|,$$

where $|\pm\rangle = (|0\rangle \pm |1\rangle)/\sqrt{2}$. Choosing $|\psi_0\rangle = \cos\frac{\theta}{2}|+\rangle + e^{i\varphi}\sin\frac{\theta}{2}|-\rangle$, $|\psi_0^\perp\rangle = \sin\frac{\theta}{2}|+\rangle - e^{i\varphi}\cos\frac{\theta}{2}|-\rangle$, one gets

$$S(\omega) = \frac{1}{4} \left| F(-\omega)e^{i\varphi}\cos^2\frac{\theta}{2} - F^*(\omega)e^{-i\varphi}\sin^2\frac{\theta}{2} \right|^2,$$

which, upon averaging over the angles θ, φ on the Bloch sphere, leads to

$$S(\omega) = \frac{1}{12} (|F(\omega)|^2 + |F(-\omega)|^2).$$

Let us now consider a Gaussian pulse for performing the quantum gate, $f(t) = [\alpha/(\sqrt{2\pi}\tau_p)]e^{-\frac{1}{2}(t/\tau_p)^2}$, where τ_p is the gate duration, while α is the angle determining the rotation. The function $|F(\omega)|^2$ that carries all the needed information about spectral properties of the system's dynamics may be approximately written as

$$|F_\pm(\omega)|^2 \approx \alpha^2 e^{-\tau_p^2 \left(\omega \pm \frac{\alpha}{\sqrt{2\pi}\tau_p} \right)^2}. \quad (1.58)$$

As may be seen from (1.57) and (1.58), for a spectral density $R(\omega) \sim \omega^n$ the error scales with the gate duration as τ_p^{-n+1} and τ_p^{-n+2} at low and high temperatures, respectively. Therefore, for $n > 2$ (typical for various types of phonon reservoirs) the error grows for faster gates. Assuming the spectral density of the form $R(\omega) = R_{\text{DP}}\omega^3$ for low frequencies (as for the deformation potential coupling at low temperatures), we obtain from (1.57) and (1.58)

$$\delta = \frac{1}{12}\alpha^2 R_{\text{DP}}\tau_p^{-2}, \quad \text{at } T = 0$$

This leading order formula holds for $\delta \ll 1$. Also, if we introduce the upper cut-off, the error will be finite even for an infinitely fast gate (see Fig. 1.8); this is the ultrafast limit discussed in Sec. 1.7.1.

Thus, the phonon-induced error indeed decreases for slow driving. This could result in obtaining arbitrarily low error by choosing a suitably low gate speed. However, if the system is also subject to other types of noise this becomes impossible.⁴⁹ Indeed, assuming an additional contribution growing with rate γ_M , the total error per gate is

$$\delta = \frac{\gamma_{\text{nM}}}{\tau_p^2} + \gamma_M\tau_p, \quad \gamma_{\text{nM}} = \frac{1}{12}\alpha^2 R_{\text{DP}}, \quad \gamma_M = \frac{1}{\tau_r}, \quad (1.59)$$

where τ_r is the characteristic time of Markovian decoherence (recombination time in the excitonic case). As a result, the overall error is unavoidable and

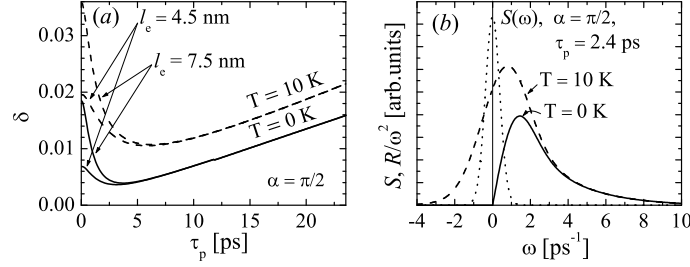


Fig. 1.8. (a) Combined Markovian and non-Markovian error for a $\alpha = \pi/2$ rotation on a qubit implemented as a confined exciton in a InAs/GaAs quantum dot, for $T = 0$ (solid lines) and $T = 10$ K (dashed lines), for two dot sizes (dot height is 20% of its diameter). The Markovian decoherence times are inferred from experimental data.⁴⁰ (b) Spectral density of the phonon reservoir $R(\omega)$ at these two temperatures and the gate profile $S(\omega)$ for $\alpha = \pi/2$.

optimization is needed. The formulas (1.59) lead to the optimal values of the form (for $T = 0$)

$$\delta_{\min} = \frac{3}{2} \left(\frac{2\alpha^2 R_{\text{DP}}}{3\tau_r^2} \right)^{1/3}, \quad \text{for } \tau_p = \left(\frac{2}{3} \alpha^2 R_{\text{DP}} \tau_r \right)^{1/3}. \quad (1.60)$$

For the specific material parameters of GaAs, the optimal gate time and minimal decoherence resulting from Eqs. (1.60) are

$$\tau_p = \alpha^{2/3} 1.47 \text{ ps}, \quad \delta_{\min} = \alpha^{2/3} 0.0035.$$

The exact solution within the proposed model, taking into account the cut-off and anisotropy (flat shape) of the dot and allowing finite temperatures, is shown in Fig. 1.8. The size-dependent cut-off is reflected by a shift of the optimal parameters for the two dot sizes: larger dots allow faster gates and lead to lower error.

It should be noted that these optimal times are longer than the limits imposed by level separation.^{48,53,54} Thus, the non-Markovian reservoir effects (dressing) seem to be the essential limitation to the gate speed. On the other hand, in the above discussion we used simple Gaussian pulses and a straightforward way of encoding the qubit. The error resulting from the phonon dynamics may be reduced by optimizing the shape of the control pulse^{55,56} or by encoding the qubit into a state of an array of QDs.⁵⁷

1.7.3. Correlation expansion

The correlation expansion technique is a standard method used for the description of quantum kinetics of interacting carriers and phonons in semiconductor systems of any dimensionality.⁵⁸ It has been successfully applied to carrier-phonon kinetics in quantum dots driven by an optical field, beyond the instantaneous excitation limit described in Sec. 1.7.1 and beyond the weak perturbation case which allows a perturbative treatment (Sec. 1.7.2).^{59–61} Compared to higher-dimensional systems, in quantum dots coherent and non-equilibrium phonons play a larger role because of the localized polaron effect. Therefore, a reliable description of the carrier phonon-kinetics in these systems requires a high enough degree of the correlation-expansion technique.⁶¹

Various implementations of this technique differ in notation and in the choice of dynamical variables. Here, let us start from the three dynamical variables x, y, z describing the carrier state, $x = \langle \sigma_x(t) \rangle, \dots$, where $\sigma_i(t) = e^{i\tilde{H}t/\hbar} \sigma_i e^{i\tilde{H}t/\hbar}$ are Pauli operators, written in the $|0\rangle, |1\rangle$ basis, in the Heisenberg picture. These three variables are the coordinates of the evolving Bloch vector, uniquely determining the reduced density matrix of the carrier subsystem according to Eq. (1.1).

From the Heisenberg equations of motion one finds the dynamical equations for these three variables,

$$\dot{x} = i\langle [H, \sigma_x] \rangle = -\Delta y - 4y \sum_{\mathbf{k}} \text{Re } B_{\mathbf{k}} - 4y \sum_{\mathbf{k}} \text{Re } y_{\mathbf{k}}, \quad (1.61)$$

and analogous for y and z (from now on, the time dependence will not be written explicitly). Obviously, this set of equations is not closed, but involves new the phonon variables $B_{\mathbf{k}} = g_{\mathbf{k}} \langle b_{\mathbf{k}} \rangle$, as well as phonon-assisted variables of the form $y_{\mathbf{k}} = g_{\mathbf{k}} \langle \langle \sigma_y b_{\mathbf{k}} \rangle \rangle = \langle \sigma_y b_{\mathbf{k}} \rangle - \langle \sigma_y \rangle \langle b_{\mathbf{k}} \rangle$. The double angular brackets, $\langle \langle \dots \rangle \rangle$, denote the correlated part of a product of operators, obtained by subtracting all possible factorizations of the product.

Next, one writes down the equations of motion for the new variables that appeared in the previous step, for instance,

$$\begin{aligned} \dot{y}_{\mathbf{k}} = i\langle [H, y_{\mathbf{k}}] \rangle = & \Delta x_{\mathbf{k}} - 2V z_{\mathbf{k}} - i\omega_{\mathbf{k}} y_{\mathbf{k}} + |g_{\mathbf{k}}|^2 (iyz + x) \\ & + 2 \sum_{\mathbf{q}} (x_{\mathbf{q}\mathbf{k}} + \tilde{x}_{\mathbf{q}\mathbf{k}}) + 4x_{\mathbf{k}} \sum_{\mathbf{q}} \text{Re } B_{\mathbf{q}} + 2x \sum_{\mathbf{q}} (B_{\mathbf{q}\mathbf{k}} + \tilde{B}_{\mathbf{q}\mathbf{k}}), \end{aligned} \quad (1.62)$$

where the new two-phonon and two-phonon-assisted variables are defined as $B_{\mathbf{q}\mathbf{k}} = g_{\mathbf{q}} g_{\mathbf{k}} \langle \langle b_{\mathbf{q}} b_{\mathbf{k}} \rangle \rangle$, $\tilde{B}_{\mathbf{q}\mathbf{k}} = g_{\mathbf{q}}^* g_{\mathbf{k}} \langle \langle b_{\mathbf{q}}^\dagger b_{\mathbf{k}} \rangle \rangle$, $x_{\mathbf{q}\mathbf{k}} = g_{\mathbf{q}} g_{\mathbf{k}} \langle \langle \sigma_x b_{\mathbf{q}} b_{\mathbf{k}} \rangle \rangle$, $\tilde{x}_{\mathbf{q}\mathbf{k}} = g_{\mathbf{q}}^* g_{\mathbf{k}} \langle \langle \sigma_x b_{\mathbf{q}}^\dagger b_{\mathbf{k}} \rangle \rangle$, etc. In the next step, one writes the equation of motion

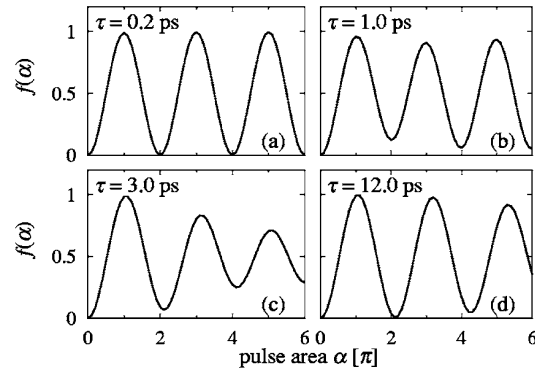


Fig. 1.9. Rabi oscillations of the exciton occupation $f = (1 + z)/2$ as a function of the nominal pulse area α , calculated using the correlation expansion at $T = 0$. Reprinted from Ref. 61, A. Krugel *et al.*, Phys. Rev. B. **73**, 035302 (2006), ©American Physical Society 2006.

for these new variables, introducing three-phonon variables. It is clear that the resulting hierarchy of equations is infinite and has to be truncated at a certain level. Here we do this by setting all the correlated parts of the three-phonon and three-phonon assisted variables equal to zero. This amounts to neglecting the correlations involving three or more phonons or, physically, to neglecting three-phonon processes (that is, emission or absorption of three or more phonons within the memory time of the phonon reservoir, which is of order of 1 ps). The motivation for this procedure is that higher order correlations should play a decreasing role in the dynamics. From the equations of motion it is also clear that such higher order correlations develop in higher orders with respect to the coupling constants $g_{\mathbf{k}}$.

As an example of an application of this technique, Fig. 1.9 shows the results for the Rabi oscillations of a coherently driven exciton (see Sec. 1.4) interacting with phonons.⁶⁰ An interesting feature of this result is that the quality of oscillations decreases for moderate pulse durations but then increases again for longer pulses. This can be understood (using the perturbative approach of Sec. 1.7.2) in terms of a resonance between the oscillations of the charge distribution and the phonon modes.⁶²

1.8. Conclusion

This chapter presented an overview of some recent results related to optical control and decoherence of carriers in semiconductor quantum dots. The

problems discussed here are of interest not only from the scientific point of view but are also important for possible applications of nanostructure-based devices in the field of nano-electronics, optoelectronics and spintronics.^{63,64}

Obviously, a chapter of limited length cannot give an exhaustive review of this broad and rapidly developing field. Consequently, the goal of the present review was rather to give an introduction to the field rather than a complete, encyclopedic account of all the achievements. In particular, the two level (or few-level) model on which the presented discussion was based, is obviously merely an approximation to the complex semiconductor system. In fact, any interaction of the confined carriers with the external driving fields not only leads to the desired quantum transitions but also can induce some unwanted ones. If both the desired and unwanted transitions have a discrete nature (e.g., the exciton vs. biexciton transition in a QD) the latter may be suppressed by a suitable choice of control pulses.^{53,54} A more demanding problem of transitions involving the macroscopic phonon continuum is treated in Ref.⁵⁶

Another class of experiments and theories that are not covered by this review concerns optical methods for coherent spin control in QDs. The capability of encoding and manipulating information at the single-spin level is of great importance for spintronic and quantum information processing applications. Recent experimental progress includes the generation⁶⁵ and optical control^{66,67} of the spin coherence together with a possible read-out of the state of a single confined spin in a QD system.⁶⁸ It was also demonstrated that spin states in QDs may be prepared with high fidelity (exceeding 99.8%) by optical coupling of electronic spin states. This was done by resonant excitation of the trion transition in the presence of small heavy-light hole mixing.⁶⁹ Corresponding to these achievements, a range of schemes for optical spin control has been proposed theoretically.⁷⁰⁻⁷⁵ These schemes are based on quantum-optical procedures, exploiting the structure of selection rules in a QD discussed in this chapter. In particular, the spin rotation is performed by coupling of a single electron state to a trion state. Since the spin control is achieved by means of spin-dependent charge evolution these procedures result in phonon-induced dephasing that may be described using the methods described here.⁷⁶ An introductory review of optical spin control in QDs is given elsewhere.⁷⁷

References

1. M. A. Reed, Quantum dots, *Scientific American*. **3**, 40, (1993).

2. L. Jacak, P. Hawrylak, and A. Wojs, *Quantum Dots*. (Springer Verlag, Berlin, 1998).
3. D. Bimberg, M. Grundmann, and N. Ledentsov, *Quantum Dot Heterostructures*. (Wiley, Chichester, 1999).
4. P. M. Petroff and S. P. Denbaars, *Superlattices and Microstructures*. **15**, 15, (1994).
5. P. W. Fry, I. E. Itskevich, D. J. Mowbray, M. S. Skolnick, J. J. Finley, J. A. Baker, E. P. O'Reilly, L. R. Wilson, I. A. Larkin, P. A. Maksym, M. Hopkinson, M. Al-Khafaji, J. P. R. David, A. G. Cullis, G. Hill, and J. C. Clark, Inverted electron-hole alignment in inas-gaas self-assembled quantum dots, *Phys. Rev. Lett.* **84**, 733, (2000).
6. A. Wójs, P. Hawrylak, S. Fafard, and L. Jacak, Electronic structure and magneto-optics of self-assembled quantum dots, *Phys. Rev. B*. **54**, 5604, (1996).
7. A. Wójs and P. Hawrylak, Negatively charged magneto-excitons in quantum dots, *Phys. Rev. B*. **51**, 10880, (1995).
8. P. Hawrylak, A. Wójs, and J. A. Brum, Magneto-excitons and correlated electrons in quantum dots in a magnetic field, *Phys. Rev. B*. **54**, 11397, (1996).
9. G. Chen, N. H. Bonadeo, D. G. Steel, D. Gammon, D. S. Katzer, D. Park, and S. L. J, Optically induced entanglement of excitons in a single quantum dot, *Science*. **289**, 1906, (2000).
10. A. Hartmann, Y. Ducommun, E. Kapon, U. Hohenester, and E. Molinari, Few-particle effects in semiconductor quantum dots: Observation of multi-charged excitons, *Phys. Rev. Lett.* **84**, 5648, (2000).
11. V. M. Axt and T. Kuhn, Femtosecond spectroscopy in semiconductors: a key to coherences, correlations and quantum kinetics, *Rep. Prog. Phys.* **67**, 433, (2004).
12. H. J. Krenner, S. Stuffer, M. Sabathil, E. C. Clark, P. Ester, M. Bichler, G. Abstreiter, J. J. Finley, and A. Zrenner, Recent advances in quantum information processing based on quantum dot nanostructures, *New J. Phys.* **7**, 184, (2005).
13. T. H. Stievater, X. Li, D. G. Steel, D. Gammon, D. S. Katzer, D. Park, C. Piermarocchi, and L. J. Sham, Rabi oscillations of excitons in single quantum dots, *Phys. Rev. Lett.* **87**, 133603, (2001).
14. H. Htoon, T. Takagahara, D. Kulik, O. Baklenov, A. L. Holmes Jr., and C. K. Shih, Interplay of Rabi oscillations and quantum interference in semiconductor quantum dots, *Phys. Rev. Lett.* **88**, 087401, (2002).
15. A. Zrenner, E. Beham, S. Stuffer, F. Findeis, M. Bichler, and G. Abstreiter, Coherent properties of a two-level system based on a quantum-dot photodiode, *Nature*. **418**, 612, (2002).
16. S. Stuffer, P. Ester, A. Zrenner, and M. Bichler, Quantum optical properties of a single $\text{In}_x\text{Ga}_{1-x}\text{As}$ -GaAs quantum dot two-level system, *Phys. Rev. B*. **72**,R121301, (2005).
17. P. Borri, W. Langbein, S. Schneider, U. Woggon, R. L. Sellin, D. Ouyang, and D. Bimberg, Rabi oscillations in the excitonic ground-state transition of

- InGaAs quantum dots, *Phys. Rev. B.* **66**, R081306, (2002).
18. S. Stuffer, P. Machnikowski, P. Ester, M. Bichler, V. M. Axt, T. Kuhn, and A. Zrenner, Two-photon Rabi oscillations in a single InAs/GaAs quantum dot, *Phys. Rev. B.* **73**, 125304, (2006).
 19. T. Unold, K. Mueller, C. Lienau, T. Elsaesser, and A. D. Wieck, Optical Stark effect in a quantum dot: ultrafast control of single exciton polarizations, *Phys. Rev. Lett.* **92**, 157401, (2004).
 20. S. M. de Vasconcellos, S. Stuffer, S.-A. Wegner, P. Ester, A. Zrenner, and M. Bichler, Quantum interferences of a single quantum dot in the case of detuning, *Phys. Rev. B.* **74**, 081304, (2006).
 21. S. Stuffer, P. Ester, A. Zrenner, and M. Bichler, Ramsey fringes in an electric-field-tunable quantum dot system, *Phys. Rev. Lett.* **96**, 037402, (2006).
 22. N. N. Bonadeo, J. Erland, D. Gammon, D. S. Katzer, D. Park, and D. G. Steel, Coherent optical control of the quantum state of a single quantum dot, *Science.* **282**, 1473, (1998).
 23. H. Kamada, H. Gotoh, J. Temmyo, T. Takagahara, and H. Ando, Exciton Rabi oscillation in a single quantum dot, *Phys. Rev. Lett.* **87**, 246401, (2001).
 24. P. Machnikowski, Manifestation of fundamental quantum complementarities in time-domain interference experiments with quantum dots: A theoretical analysis, *Phys. Rev. B.* **72**, 205332, (2006).
 25. X. Li, Y. Wu, D. Steel, D. Gammon, T. Stievater, D. Katzer, D. Park, C. Piermarocchi, and L. Sham, An all-optical quantum gate in a semiconductor quantum dot, *Science.* **301**, 809, (2003).
 26. M. A. Nielsen and I. L. Chuang, *Quantum Computation and Quantum Information.* (Cambridge University Press, Cambridge, 2000).
 27. T. Unold, K. Mueller, C. Lienau, T. Elsaesser, and A. D. Wieck, Optical control of excitons in a pair of quantum dots coupled by dipole-dipole interaction, *Phys. Rev. Lett.* **94**, 137404, (2005).
 28. M. O. Scully and M. S. Zubairy, *Quantum Optics.* (Cambridge University Press, Cambridge, 1997).
 29. L. Allen and J. H. Eberly, *Optical resonance and two-level atoms.* (Dover, New York, 1987).
 30. A. Messiah, *Quantum Mechanics.* (North-Holland, Amsterdam, 1966).
 31. G. Jaeger, A. Shimony, and L. Vaidman, Two interferometric complementarities, *Phys. Rev. A.* **51**, 54, (1995).
 32. B.-G. Englert, Fringe visibility and which-way information: an inequality, *Phys. Rev. Lett.* **77**, 2154, (1996).
 33. W. K. Wootters and W. H. Zurek, Complementarity in the double-slit experiment: Quantum nonseparability and a quantitative statement of the Bohr's principle, *Phys. Rev. D.* **19**, 473, (1979).
 34. G. D. Mahan, *Many-Particle Physics.* (Kluwer, New York, 2000).
 35. H. Haken, *Quantum Field Theory of Solids. An Introduction.* (North-Holland, Amsterdam, 1976).
 36. A. Grodecka, L. Jacak, P. Machnikowski, and K. Roszak. Phonon impact on the coherent control of quantum states in semiconductor quantum dots. In P. A. Ling (ed.), *Quantum Dots: Research Developments*, p. 47. Nova

- Science, NY, (2005). Preprint cond-mat/0404364.
37. L. Jacak, P. Machnikowski, J. Krasnyj, and P. Zoller, Coherent and incoherent phonon processes in artificial atoms, *Eur. Phys. J. D.* **22**, 319, (2003).
 38. A. Vagov, V. M. Axt, and T. Kuhn, Impact of pure dephasing on the non-linear optical response of single quantum dots and dot ensembles, *Phys. Rev. B.* **67**, 115338, (2003).
 39. A. Vagov, V. M. Axt, T. Kuhn, W. Langbein, P. Borri, and U. Woggon, Non-monotonous temperature dependence of the initial decoherence in quantum dots, *Phys. Rev. B.* **70**, R201305, (2004).
 40. P. Borri, W. Langbein, S. Schneider, U. Woggon, R. L. Sellin, D. Ouyang, and D. Bimberg, Ultralong dephasing time in InGaAs quantum dots, *Phys. Rev. Lett.* **87**, 157401, (2001).
 41. P. Machnikowski and L. Jacak, Damping of Rabi oscillations in quantum dots due to lattice dynamics, *Semicond. Sci. Technol.* **19**, S299, (2004).
 42. W. Schäfer and M. Wegener, *Semiconductor Optics and Transport Phenomena*. (Springer, Berlin, 2002).
 43. A. Vagov, V. M. Axt, and T. Kuhn, Electron-phonon dynamics in optically excited quantum dots: Exact solution for multiple ultrashort laser pulses, *Phys. Rev. B.* **66**, 165312, (2002).
 44. K. Roszak and P. Machnikowski, “Which path” decoherence in quantum dot experiments, *Phys. Lett. A.* **351**, 251, (2006).
 45. B. Krummheuer, V. M. Axt, and T. Kuhn, Theory of pure dephasing and the resulting absorption line shape in semiconductor quantum dots, *Phys. Rev. B.* **65**, 195313, (2002).
 46. M. Bayer and A. Forchel, Temperature dependence of the homogeneous linewidth in $\text{In}_{0.60}\text{Ga}_{0.40}\text{As}/\text{GaAs}$ self-assembled quantum dots, *Phys. Rev. B.* **65**, R041308, (2002).
 47. C. Cohen-Tannoudji, J. Dupont-Roc, and G. Grynberg, *Atom-Photon Interactions*. (Wiley-Interscience, New York, 1998).
 48. E. Biolatti, R. C. Iotti, P. Zanardi, and F. Rossi, Quantum information processing with semiconductor macroatoms, *Phys. Rev. Lett.* **85**, 5647, (2000).
 49. R. Alicki, M. Horodecki, P. Horodecki, R. Horodecki, L. Jacak, and P. Machnikowski, Optimal strategy for a single-qubit gate and trade-off between opposite types of decoherence, *Phys. Rev. A.* **70**, R010501, (2004).
 50. P. Machnikowski, V. M. Axt, and T. Kuhn, Quantum information encoding in dressed qubits, *Phys. Rev. B.* **75**, 052330, (2007).
 51. D. Pines and P. Nozières, *The Theory of Quantum Liquids*. (Addison-Wesley, Redwood, 1989).
 52. R. Alicki, M. Horodecki, P. Horodecki, and R. Horodecki, Dynamical description of quantum computing: generic nonlocality of quantum noise, *Phys. Rev. A.* **65**, 062101, (2002).
 53. Pochung Chen, C. Piermarocchi, and L. J. Sham, Control of exciton dynamics in nanodots for quantum operations, *Phys. Rev. Lett.* **87**, 067401, (2001).
 54. C. Piermarocchi, Pochung Chen, Y. S. Dale, and L. J. Sham, Theory of fast quantum control of exciton dynamics in semiconductor quantum dots, *Phys. Rev. B.* **65**, 075307, (2002).

55. U. Hohenester and G. Stadler, Quantum control of electron-phonon scatterings in artificial atoms, *Phys. Rev. Lett.* **92**, 196801, (2004).
56. V. M. Axt, P. Machnikowski, and T. Kuhn, Reducing decoherence of the confined exciton state in a quantum dot by pulse-sequence driving, *Phys. Rev. B.* **71**, 155305, (2005).
57. A. Grodecka and P. Machnikowski, Partly noiseless encoding of quantum information in quantum dot arrays against phonon-induced pure dephasing, *Phys. Rev. B.* **73**, 125306, (2006).
58. F. Rossi and T. Kuhn, Theory of ultrafast phenomena in photoexcited semiconductors, *Rev. Mod. Phys.* **74**, 895, (2002).
59. J. Förstner, C. Weber, J. Danckwerts, and A. Knorr, Phonon-assisted damping of Rabi oscillations in semiconductor quantum dots, *Phys. Rev. Lett.* **91**, 127401, (2003).
60. A. Krügel, V. M. Axt, T. Kuhn, P. Machnikowski, and A. Vagov, The role of acoustic phonons for Rabi oscillations in semiconductor quantum dots, *Appl. Phys. B.* **81**, 897, (2005).
61. A. Krügel, V. M. Axt, and T. Kuhn, Back action of nonequilibrium phonons on the optically induced dynamics in semiconductor quantum dots, *Phys. Rev. B.* **73**, 035302, (2006).
62. P. Machnikowski and L. Jacak, Resonant nature of phonon-induced damping of Rabi oscillations in quantum dots, *Phys. Rev. B.* **69**, 193302, (2004).
63. M. Skolnick and D. Mowbray, Self-assembled semiconductor quantum dots: Fundamental physics and device applications, *Annu. Rev. Mater. Res.* **34**, 181, (2004).
64. P. Bhattacharya, S. Ghosh, and A. Stiff-Roberts, Quantum dot optoelectronic devices, *Annu. Rev. Mater. Res.* **34**, 1, (2004).
65. M. V. G. Dutt, Jun-Cheng, B. Li, X. Xu, X. Li, P. R. Berman, D. G. Steel, A. S. Bracker, D. Gammon, S. E. Economou, Ren-Bao-Liu, and L. J. Sham, Stimulated and spontaneous optical generation of electron spin coherence in charged GaAs quantum dots, *Phys. Rev. Lett.* **94**, 227403, (2005).
66. A. Greilich, R. Oulton, E. A. Zhukov, I. A. Yugova, D. R. Yakovlev, M. Bayer, A. Shabaev, A. L. Efros, V. Merkulov, V. Stavarache, D. Reuter, and A. Wieck, Optical control of spin coherence in singly charged (In,Ga)As/GaAs quantum dots, *Phys. Rev. Lett.* **96**, 227401, (2006).
67. M. V. G. Dutt, J. Cheng, Y. Wu, X. Xu, D. G. Steel, A. S. Bracker, D. Gammon, S. E. Economou, R.-B. Liu, and L. J. Sham, Ultrafast optical control of electron spin coherence in charged GaAs quantum dots, *Phys. Rev. B.* **74**, 125306, (2006).
68. M. Atatüre, J. Dreiser, A. Badolato, and A. Imamoglu, Observation of Faraday rotation from a single confined spin, *Nature Physics.* **3**, 101, (2007).
69. M. Atatüre, J. Dreiser, A. Badolato, A. Hogege, K. Karrai, and A. Imamoglu, Quantum-dot spin-state preparation with near-unity fidelity, *Science.* **312**, 551, (2006).
70. E. Pazy, E. Biolatti, T. Calarco, I. D'Amico, P. Zanardi, F. Rossi, and P. Zoller, Spin-based optical quantum gates via Pauli blocking in semiconductor quantum dots, *Europhys. Lett.* **62**, 175, (2003).

71. T. Calarco, A. Datta, P. Fedichev, E. Pazy, and P. Zoller, Spin-based all-optical quantum computation with quantum dots: understanding and suppressing decoherence, *Phys. Rev. A*. **68**, 12310, (2003).
72. F. Troiani, E. Molinari, and U. Hohenester, High-finesse optical quantum gates for electron spins in artificial molecules, *Phys. Rev. Lett.* **90**, 206802, (2003).
73. Pochung Chen, C. Piermarocchi, L. J. Sham, D. Gammon, and D. G. Steel, Theory of quantum optical control of a single spin in a quantum dot, *Phys. Rev. B*. **69**, 075320, (2004).
74. A. Nazir, B. W. Lovett, S. D. Barrett, T. P. Spiller, and G. A. D. Briggs, Selective Spin Coupling through a Single Exciton, *Phys. Rev. Lett.* **93**, 150502, (2004).
75. B. W. Lovett, A. Nazir, E. Pazy, S. D. Barrett, T. P. Spiller, G. A. D. Briggs, Quantum computing with spin qubits interacting through delocalized excitons: Overcoming hole mixing, *Phys. Rev. B*. **72**, 115324, (2005).
76. K. Roszak, A. Grodecka, P. Machnikowski, and T. Kuhn, Phonon-induced decoherence for a quantum dot spin qubit operated by raman passage, *Phys. Rev. B*. **71**, 195333, (2005).
77. P. Machnikowski, A. Grodecka, C. Weber, A. Knorr, Optical control and decoherence of spin qubits in quantum dots. Preprint arXiv:0706.0276.